Electronic Supplementary Information for

Complexes of a porphyrin-like N_4-donor Schiff-base macrocycle

Rajni K. Wilson (née Sanyal) and Sally Brooker*[a]

[a] *Department of Chemistry and MacDiarmid Institute for Advanced Materials and Nanotechnology, University of Otago, PO Box 56, Dunedin 9054, New Zealand. Fax: +64 3 479 7906. Email: sbrooker@chemistry.otago.ac.nz*

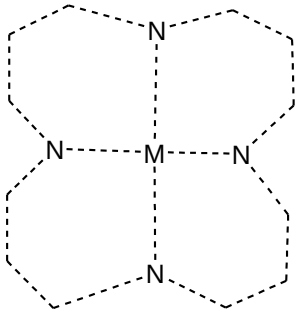

Figure S1. Basic search fragment, featuring 6666 chelate ring size of 16-membered N_4–donor macrocycles with all bonds as "any bond type", used in combination with NOT "porphyrin" NOT "corrin", to search the CSD version 5.33.

Table S1. Summary and comparison of the coordination number, geometry, imine bonds and spin state in 6666 chelate ring sized complexes of 16-membered N_4 macrocycles. Data obtained from searches of the CSD (version 5.33), with the fragment shown in Figure S1.

Metal ion (M)	Coordination number (CN)	Number of hits/geometry	Number of imines(examples)	Spin-state
Cu^{II}	4	13 x sq pl	0(2), 2(2), 4(9)	-
	5	0	-	-
	6	3 x Oh	4	-
Ni^{II}	4	23 x sq pl	0(2), 2(1), 4(20)	low-spin
	5	0	-	-
	6	6 x Oh	1(2), 2(4)	high-spin
Fe^{III}	4	0	-	-
	5	0	-	-
	6	0	-	-
Co^{II}	4	2 x Td	0	high-spin
	5	3 x sq py	4	low-spin
	6	6 x Oh	1	high-spin

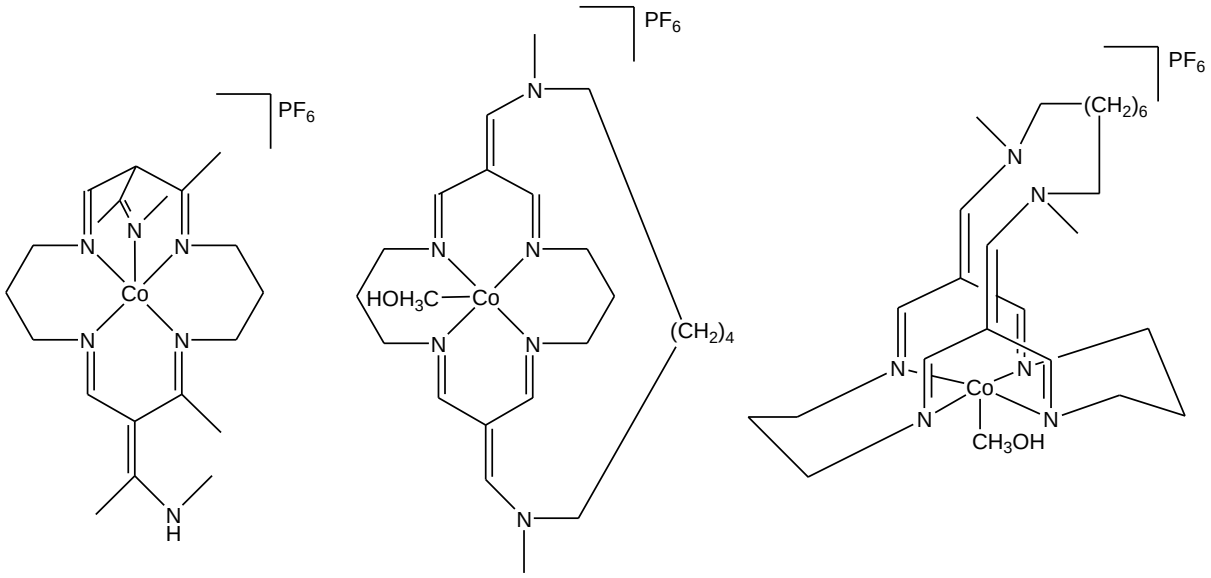

FAZPUR **RUFYIA** **NARZOV**

Figure S2. The three structurally characterized 5-CN Co^{II} complexes of 14-membered N_4 macrocyclic complexes along with their CCDC code names.[1-3]

References

1. M. L. Caste, C. J. Cairns, J. Church, W. K. Lin, J. C. Gallucci and D. H. Busch, *Inorg. Chem.*, 1987, **26**, 78-83.
2. A. G. Kolchinski, N. W. Alcock and D. H. Busch, *Inorg. Chem.*, 1997, **36**, 2754-2759.
3. A. G. Kolchinski, B. Korybut-Daszkiewicz, E. V. Rybak-Akimova, D. H. Busch, N. W. Alcock and H. J. Clase, *J. Am. Chem. Soc.*, 1997, **119**, 4160-4171.

Table S2. Fitting of microanalytical data for the crude HL^{Pr} product obtained from reactions employing (a) 1 equivalent *vs*. (b) an excess of acetic acid, relative to dialdehyde and diamine.

	%C	%H	%N
Found for stoichiometric acid addition	68.27	6.85	12.06
$C_{20}H_{24}N_4$	74.97	7.55	17.48
$C_{20}H_{24}N_4$•1.5HOAc•0.5dialdehyde	68.62	6.93	12.31
$C_{20}H_{24}N_4$•HOAc	69.45	7.42	14.72
$C_{20}H_{24}N_4$•2HOAc	65.43	7.32	12.72
Found for excess acid addition	65.04	7.58	12.79
$C_{20}H_{24}N_4$	74.97	7.55	17.48
$C_{20}H_{24}N_4$•HOAc	69.45	7.42	14.73
$C_{20}H_{24}N_4$•2HOAc	65.43	7.32	12.72

Table S3. Fitting of microanalytical data for the crude HL^{Pr} product obtained from reactions employing (a) 1 equivalent *vs*. (b) an excess of formic acid, relative to dialdehyde and diamine.

	%C	%H	%N
Found for reaction product of 1:1:1	69.22	7.10	13.65
$C_{20}H_{24}N_4$	74.97	7.55	17.48
$C_{20}H_{24}N_4$•1.2HCO_2H•0.3dialdehyde	68.83	6.75	13.59
$C_{20}H_{24}N_4$•HCO_2H	68.83	7.15	15.29
$C_{20}H_{24}N_4$•2HCO_2H	64.06	6.84	13.58
Found for excess acid addition	64.50	7.12	13.80
$C_{20}H_{24}N_4$	74.97	7.55	17.48
$C_{20}H_{24}N_4$•HCO_2H	68.83	7.15	15.29
$C_{20}H_{24}N_4$•2HCO_2H	64.06	6.84	13.58

Figure S3. ^{1}H NMR and ^{13}C NMR spectra in $CDCl_3$ of crude HL^{Pr} prepared without addition of acid.

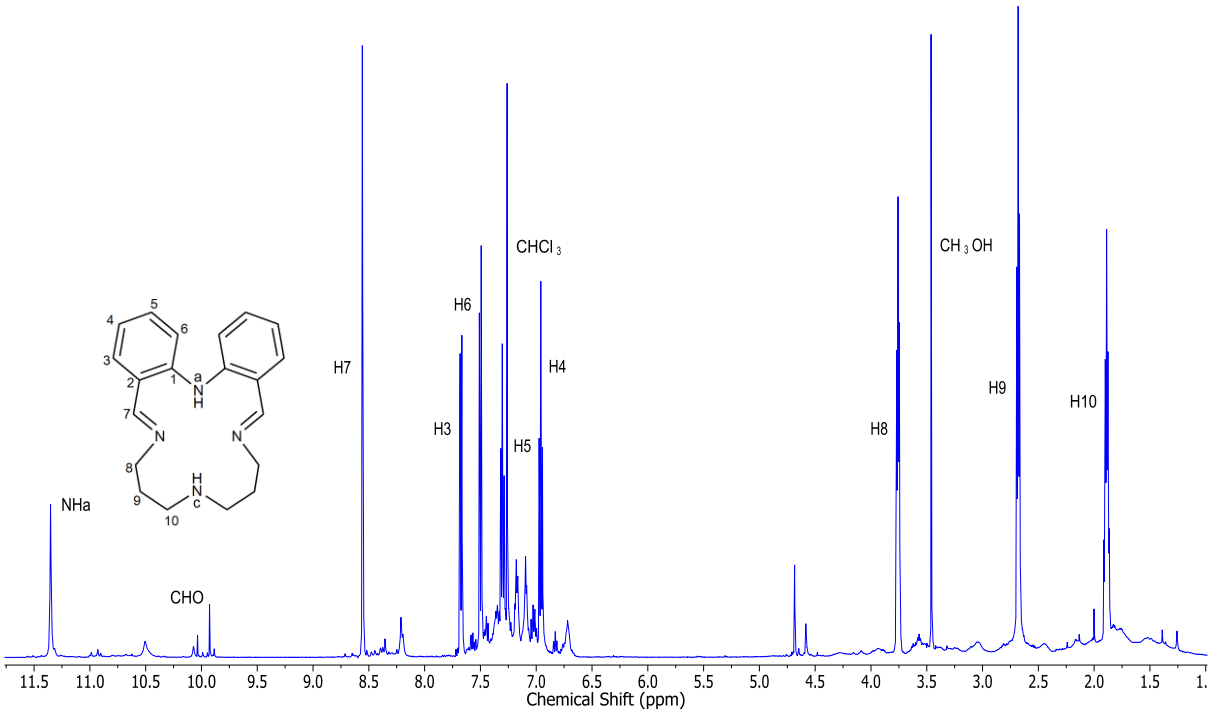

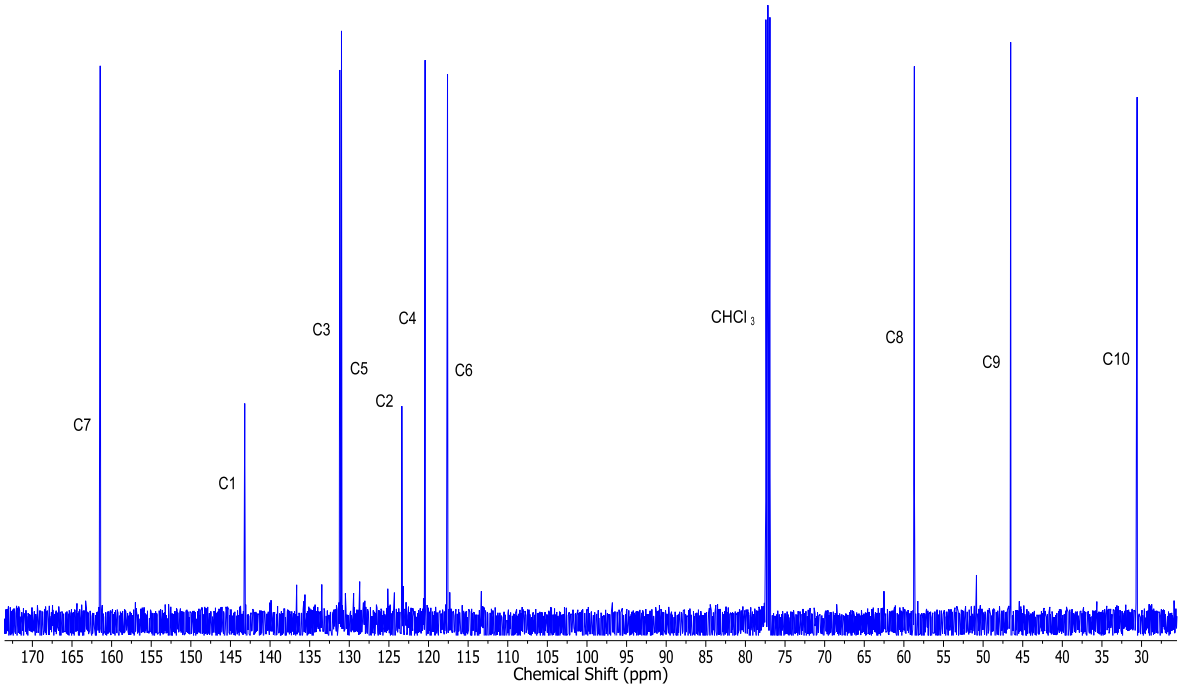

Figure S4. ^{1}H NMR and ^{13}C NMR spectra in $CDCl_3$ of HL^{Pr}•2HOAc (prepared using excess acid). Ratio of blue:red:acid signals is about 1:1:4. Strong signal at 7.26 ppm is $CHCl_3$ (black) and 1.91 ppm is CH_3CO_2H (black).

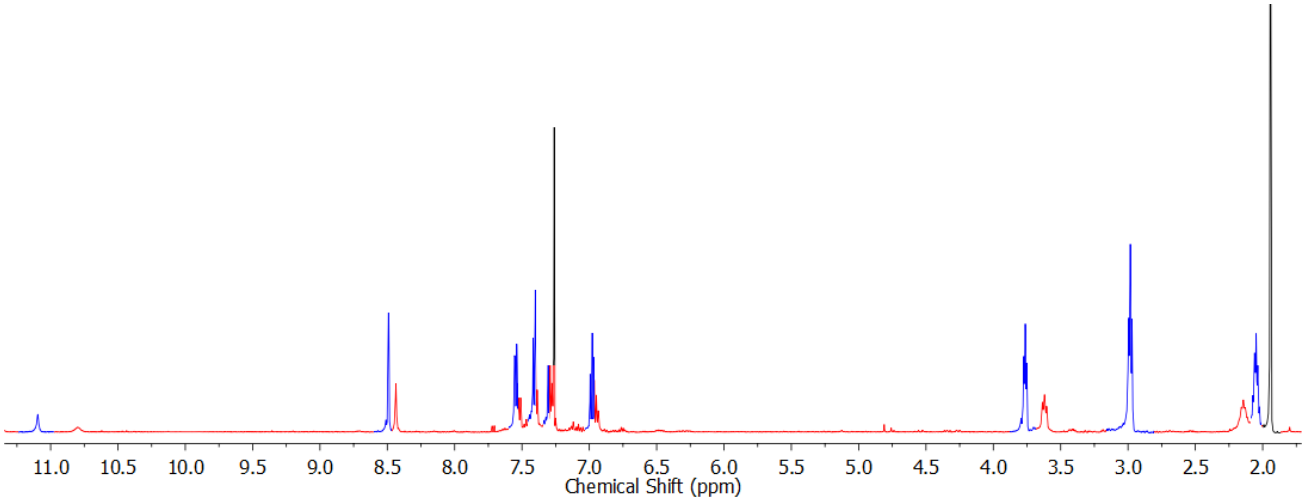

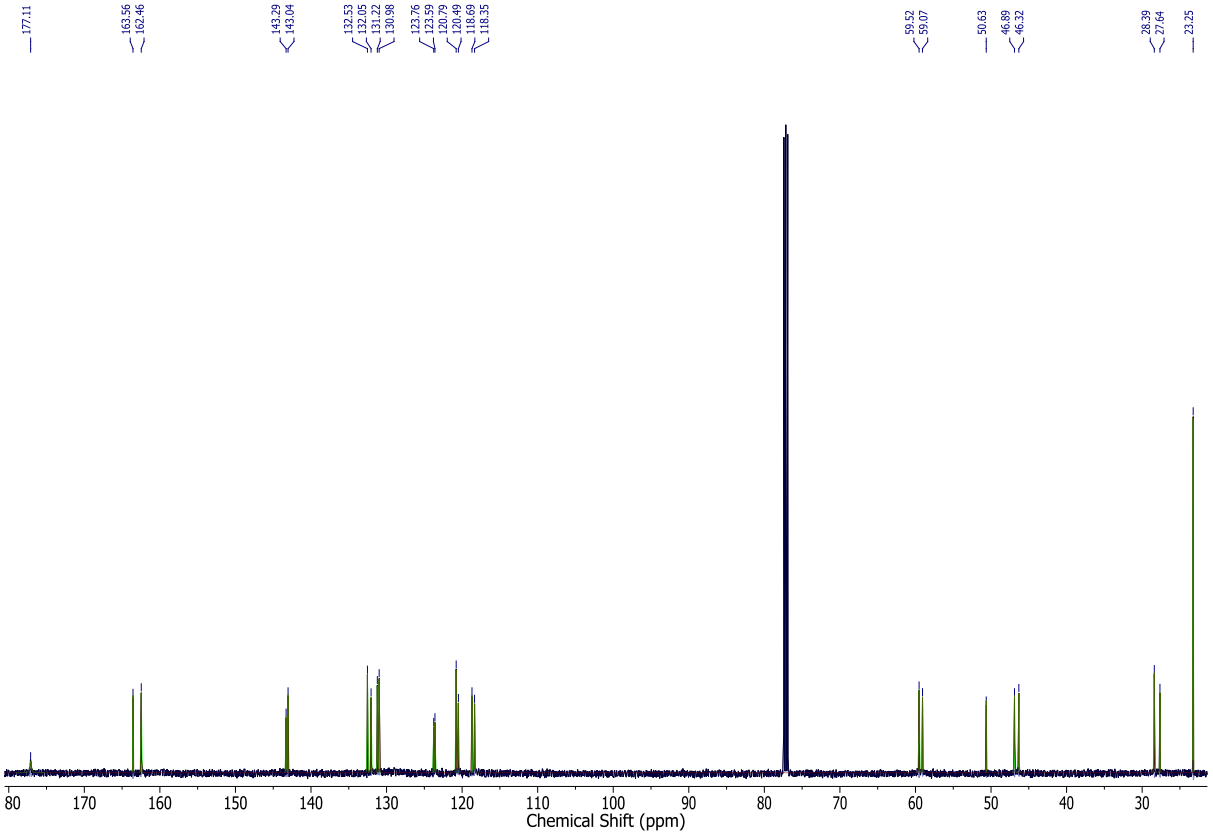

Figure S5. ^{1}H NMR and ^{13}C NMR spectra in $CDCl_3$ of HL^{Pr}•$2HCO_2H$ (prepared using excess acid). Ratio of blue:red:acid signals is about 1:1:4. Strong signal at 7.26 ppm is $CHCl_3$ (black) and 8.53 ppm is HCO_2H (black).

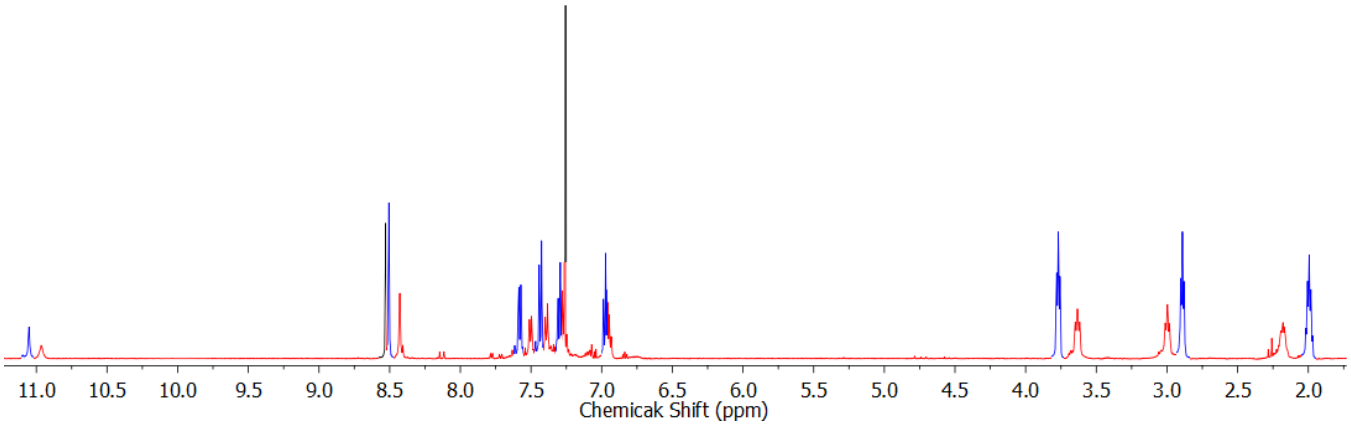

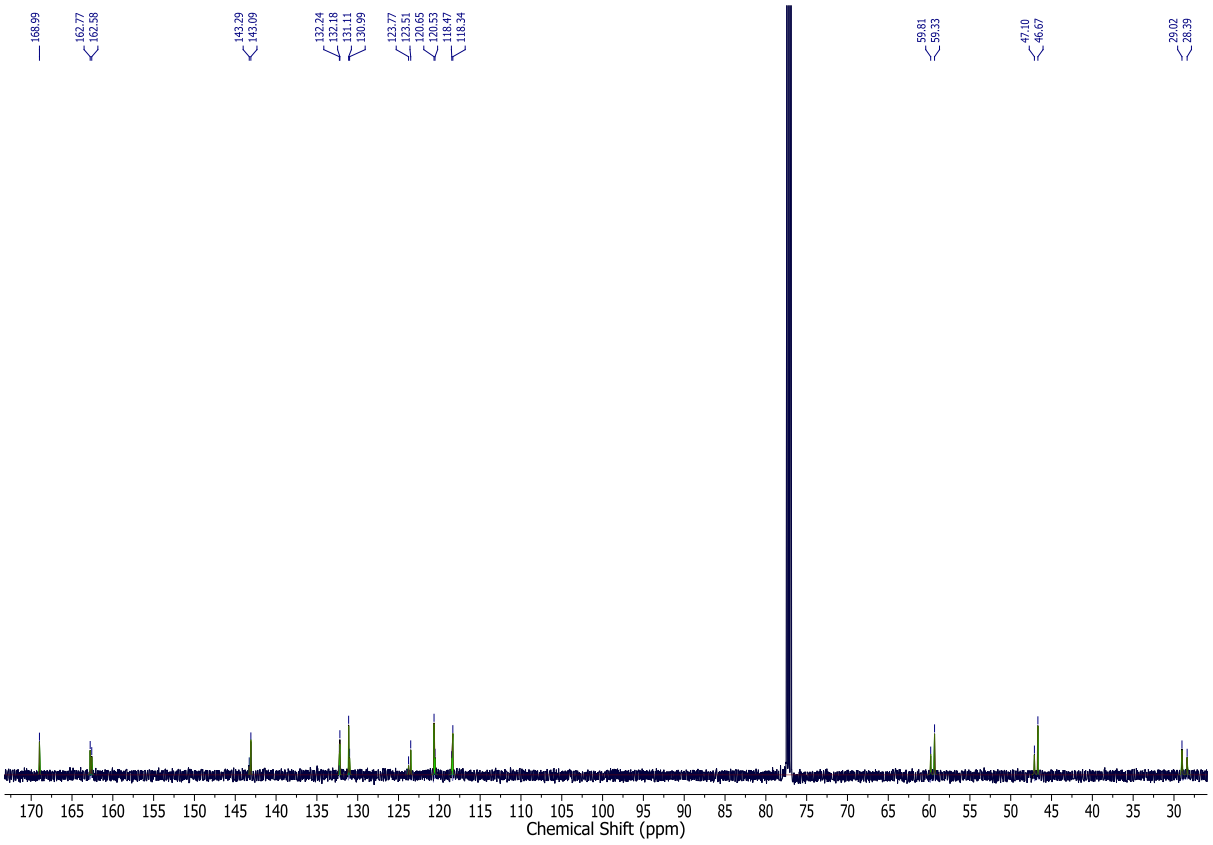

Figure S6. ^{1}H NMR spectrum of HL^{Pr}•2HOAc in CD_3OD.

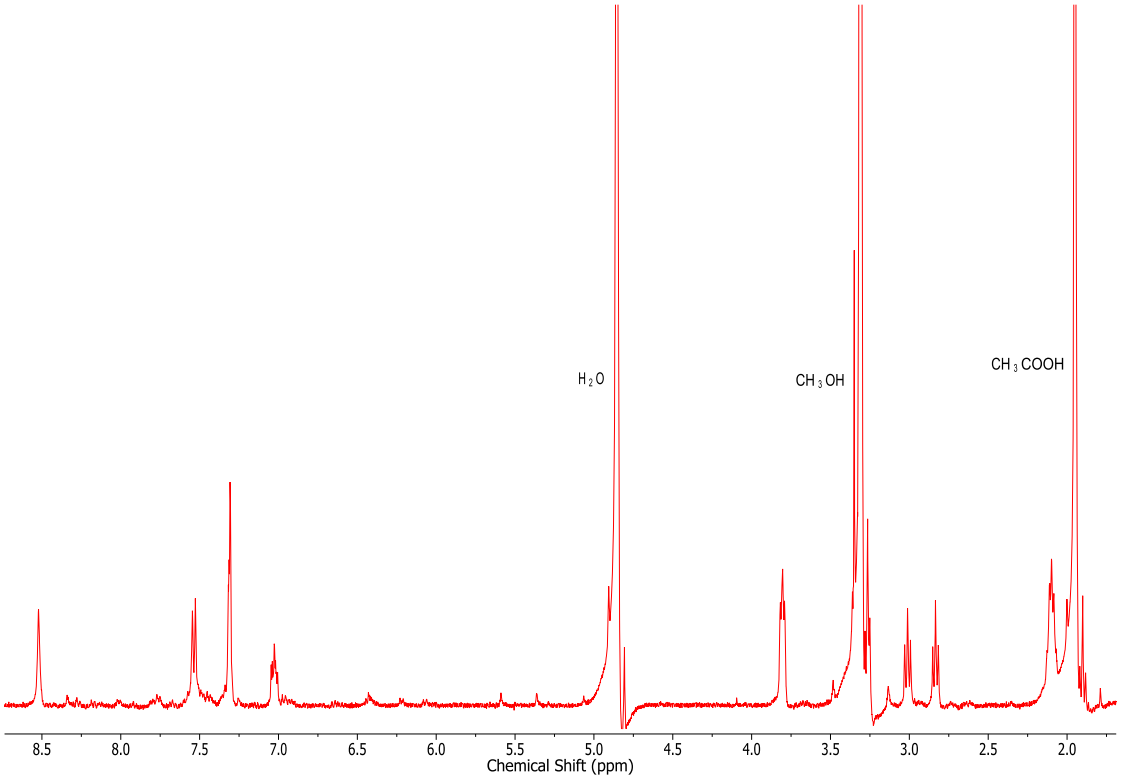

Figure S7. ^{1}H NMR spectrum of HL^{Pr}•2HCO_2H in CD_3OD.

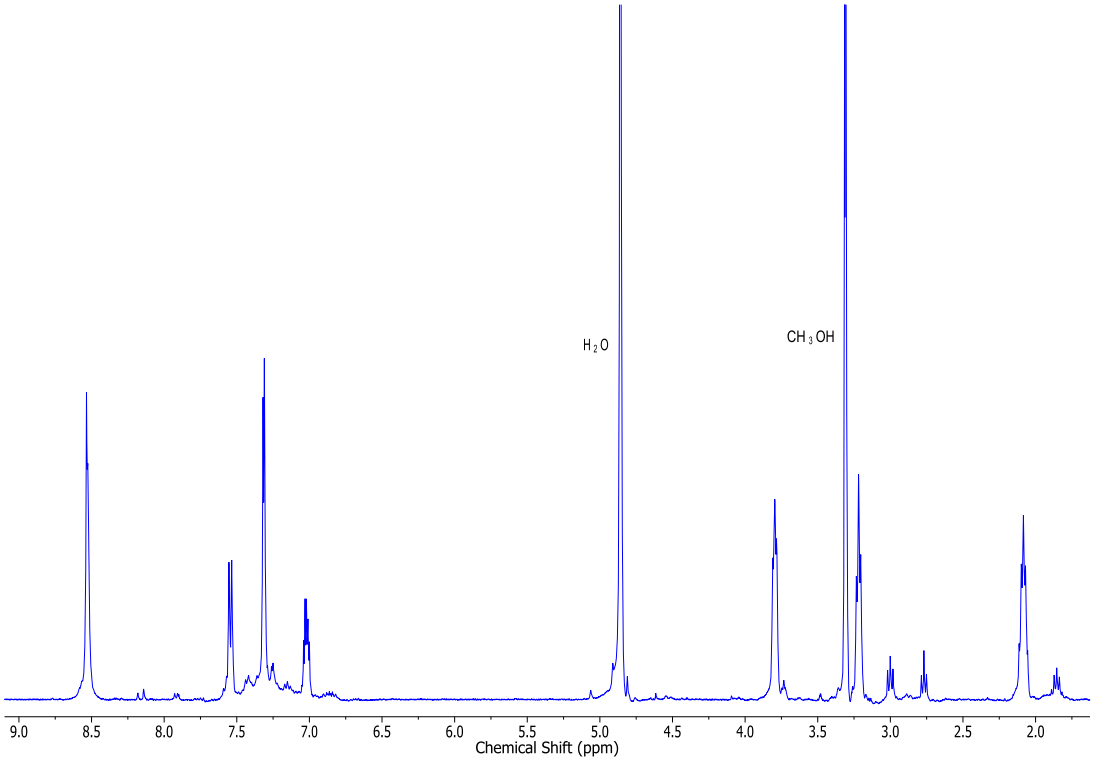

Figure S8. Comparison of the ^{1}H NMR spectra in $(CD_3)_2SO$ of $HL^{Pr}\bullet C_7H_8SO_3$ (a pale yellow solid) as: the initially obtained pale yellow suspension (top), a less milky suspension after standing overnight in the NMR tube (middle) and a pale yellow clear solution after standing in the NMR tube for 5 days (bottom). This pale yellow solid was obtained as a precipitate from the 1:1:1 reaction of dialdehyde **1**, dipropylene triamine and one equivalent of tosylic acid.

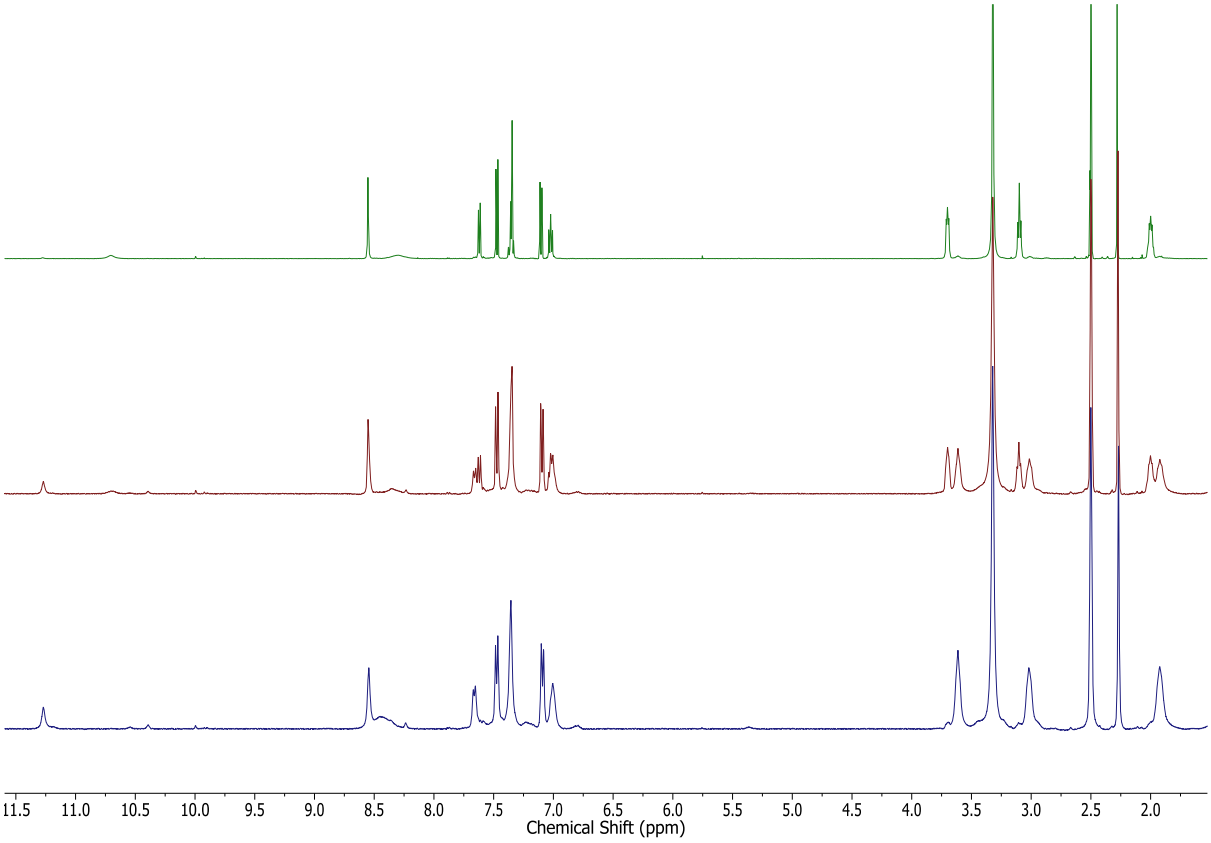

Figure S9. ^{1}H NMR spectrum suspended in $(CD_3)_2SO$ of $HL^{Pr}\bullet C_7H_8SO_3$. Red molecule is neutral overall. Ratio of blue:red:acid signals is about 1:1:1. Strong signals in black at 3.3, 2.5 and 2.3 ppm are H_2O (from DMSO), DMSO and the CH_3 group of the tosylic acid. The suspension was less milky after standing overnight in the NMR tube – after this spec was obtained.

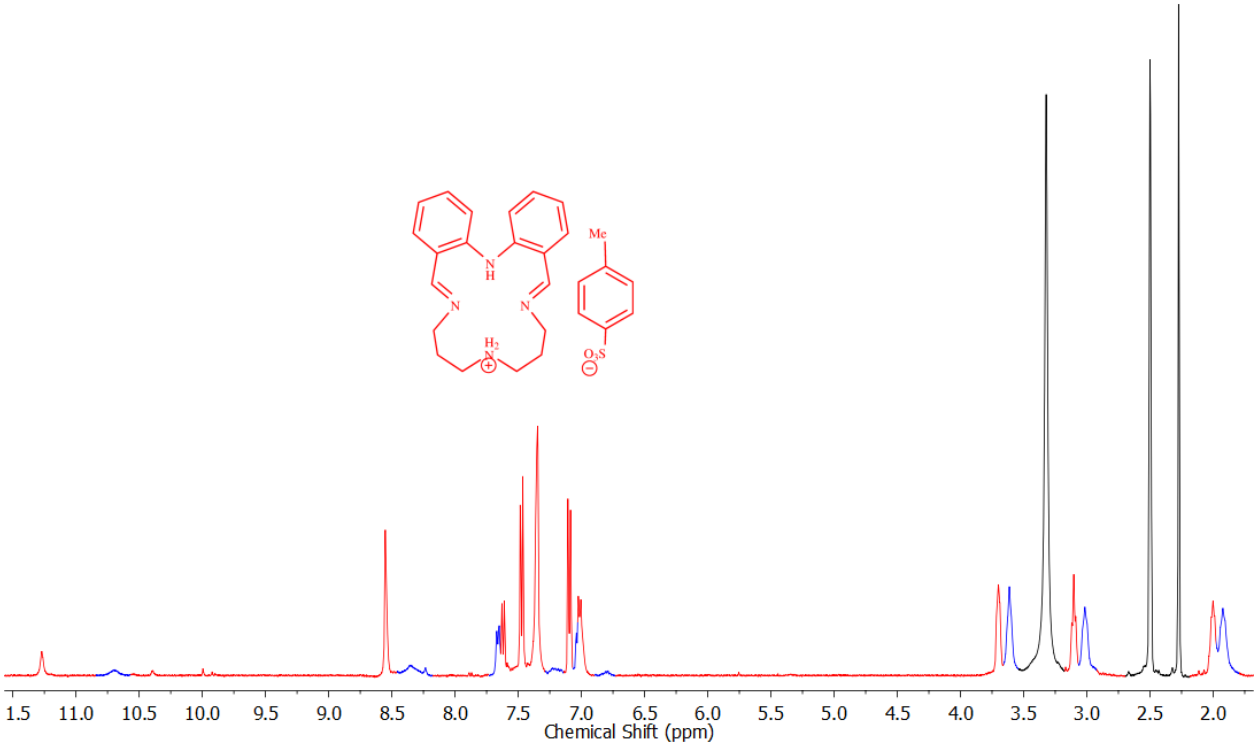

Figure S10. ^{1}H NMR and ^{13}C NMR spectra of $HL^{Pr}\bullet C_7H_8SO_3$ as a pale yellow clear solution, in $(CD_3)_2SO$, obtained after leaving the initially obtained suspension in the NMR tube for 5 days. Red molecule is neutral overall. Ratio of blue:red:acid signals is about 1:0.2:1. Strong signals in black at 3.3, 2.5 and 2.3 ppm are H_2O (from DMSO), DMSO and the CH_3 group of the tosylic acid.

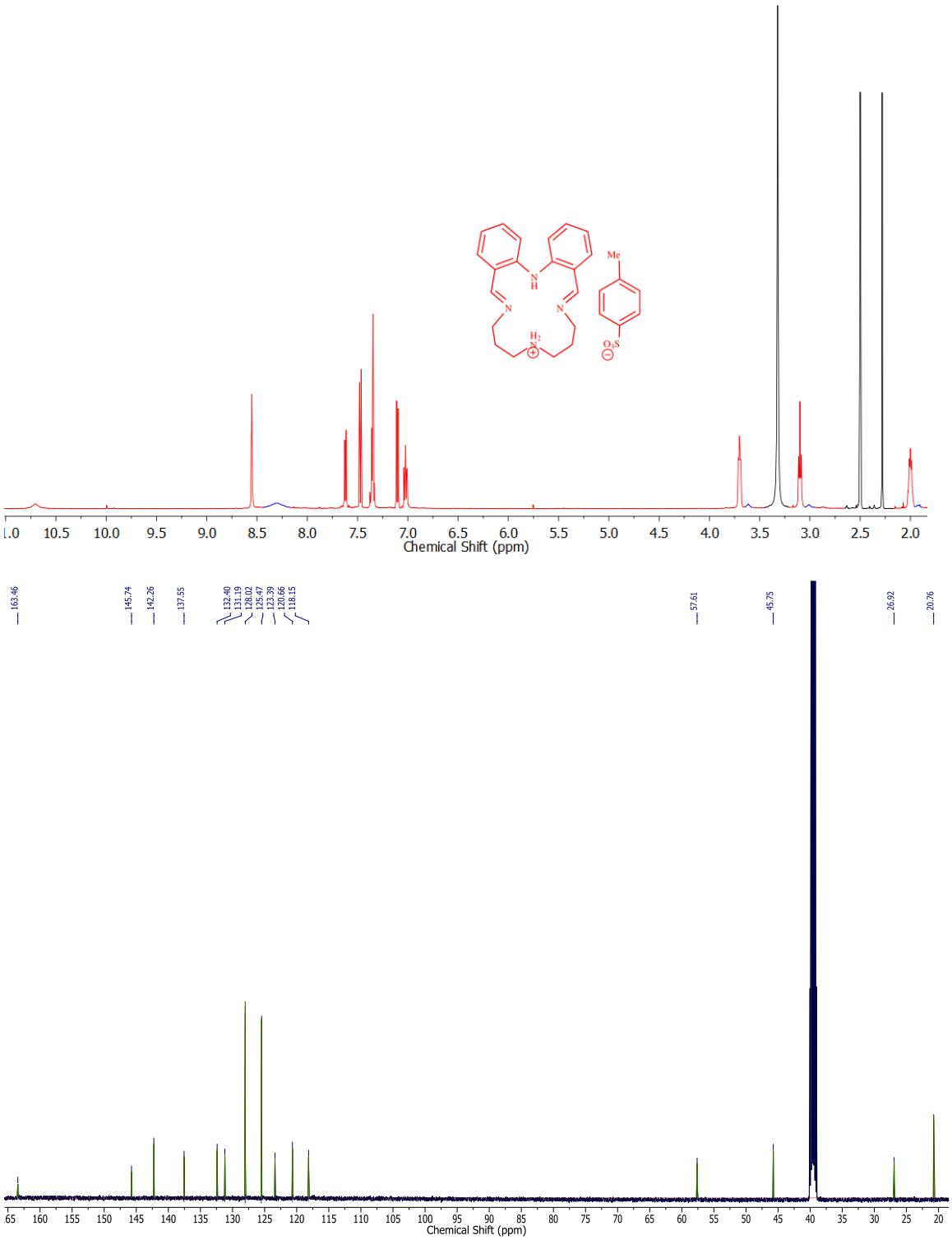

Figure S11. Comparison of the ^{1}H NMR spectra of the various HL^{Pr} product mixtures obtained from different syntheses: (bottom) the crude macrocycle HL^{Pr} (not acid catalyzed), (lower middle) HL^{Pr}•2HOAc, and (upper middle) HL^{Pr}•$2HCO_2H$ in $CDCl_3$ and (top) HL^{Pr}•$C_7H_8SO_3$ in $(CD_3)_2SO$.

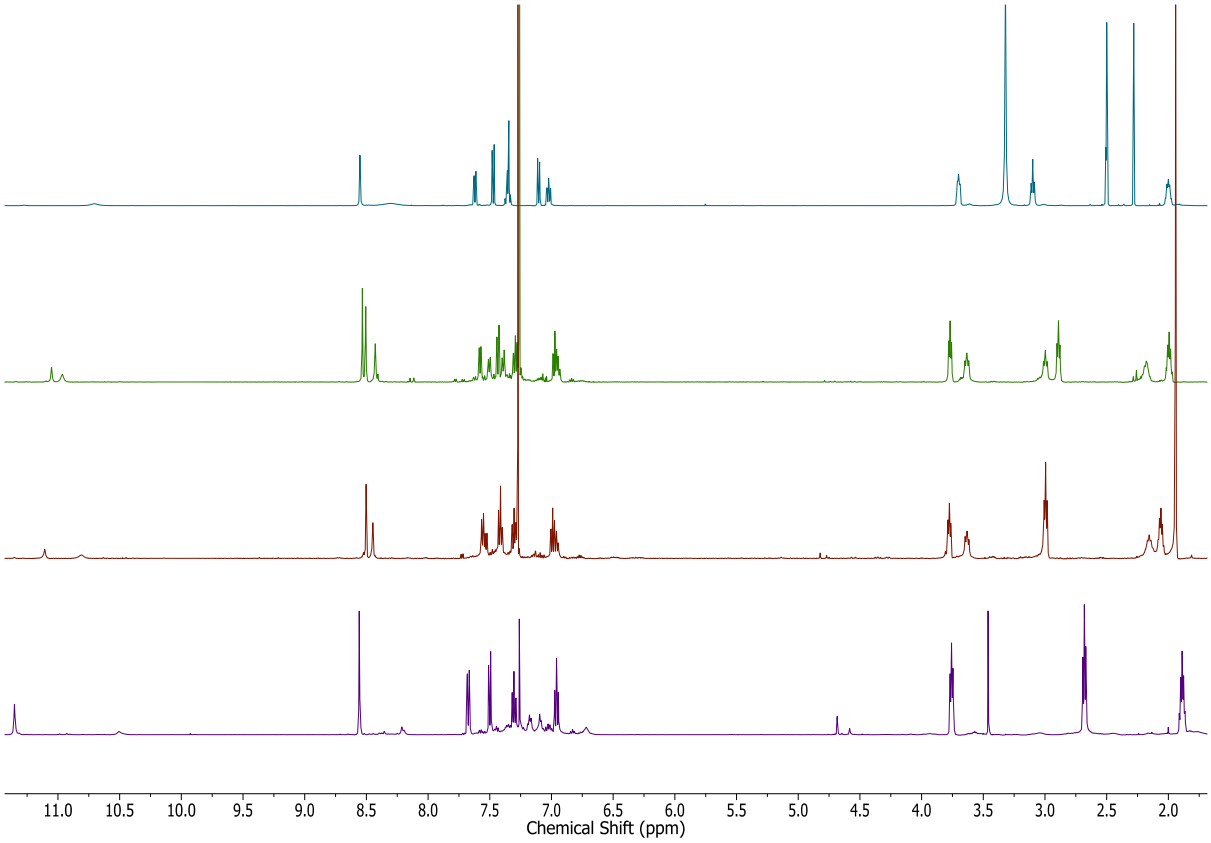

Figure S12. ^{1}H NMR spectra of HL^{Pr}•$2HCO_2H$ in $CDCl_3$ at: (top) 323, (middle) 273 and (bottom) 252 K.

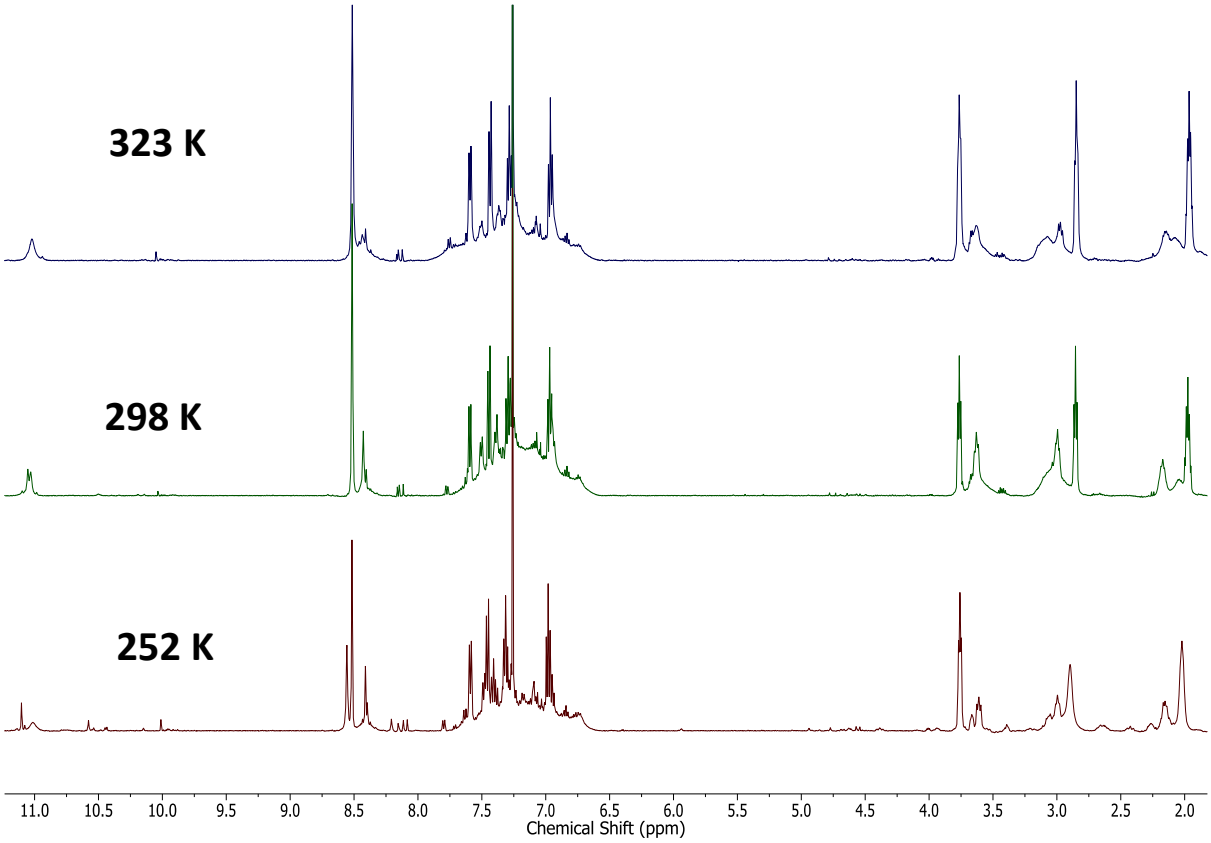

Figure S13. Comparison of the ^{1}H NMR spectra in $CDCl_3$ of: (bottom) crude HL^{Pr} (prepared without addition of acid) and (top) HL^{Pr}•$2HCO_2H$ (at 323 K).

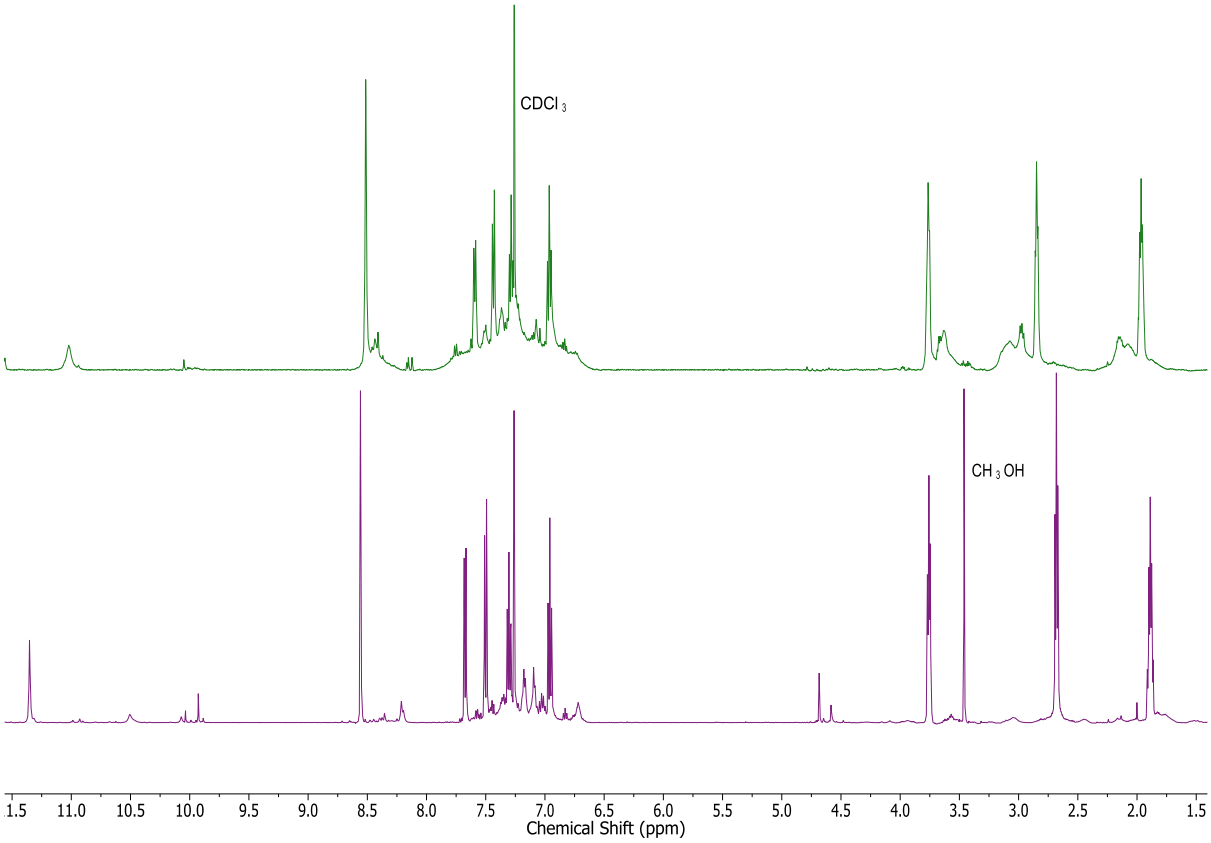

Figure S14. Comparison of the ^{1}H NMR spectra of: (bottom) HL^{Pr}•$2HCO_2H$ (at 323 K) in $CDCl_3$ and (top) HL^{Pr}•$2HCO_2H$ in CD_3OD.

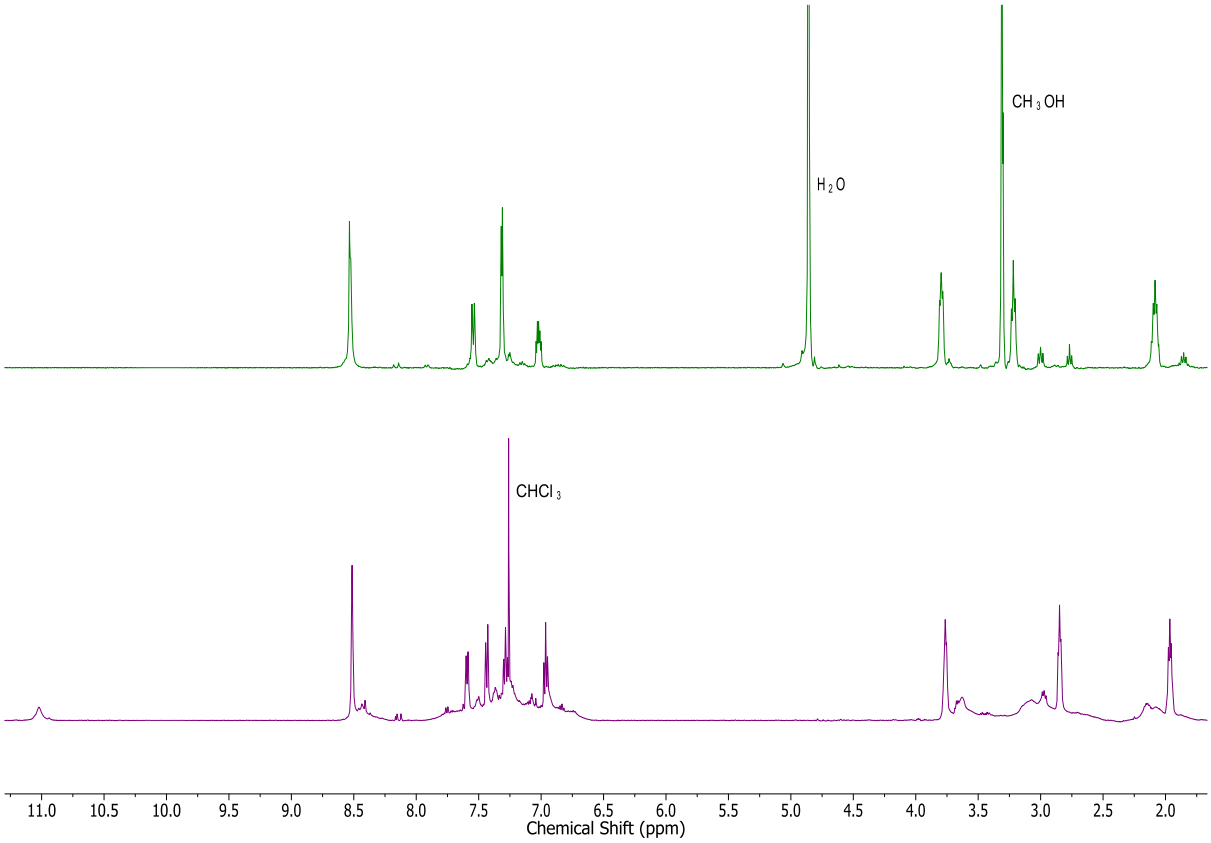

Figure S15. ^{1}H NMR spectrum in $(CD_3)_2SO$ of a bright red oil resulting from a 1:1:2 reaction of dialdehyde **1**, dipropylene triamine and tosylic acid.

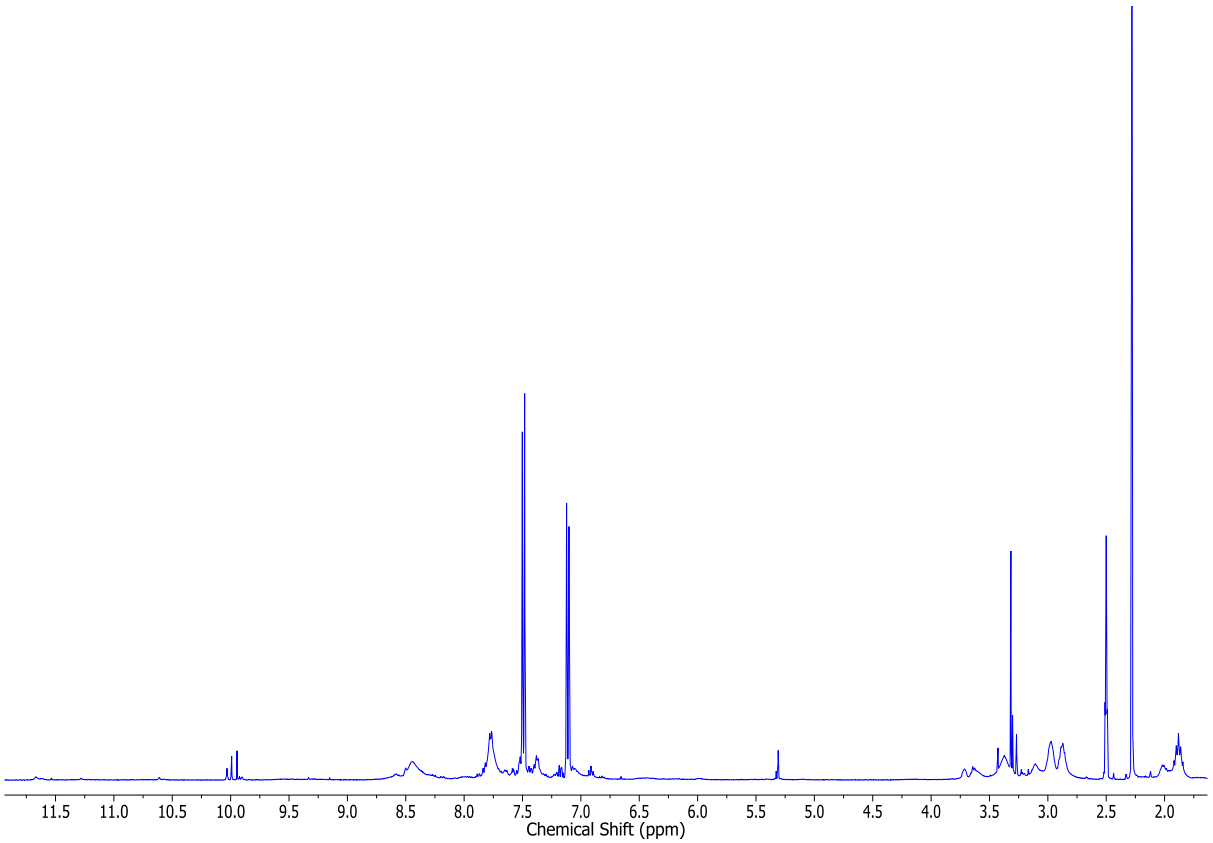

Figure S16. Comparison the ^{1}H NMR spectra of the bright red oil obtained from each of the following three 1:1:2 reactions of dialdehyde **1**, dipropylene triamine and acid: (bottom) acetic acid, (middle) formic acid and (top) tosylic acid. The acetic and formic acid reaction products were run in $CDCl_3$ whereas, due to poor solubility, that from the tosylic acid reaction was run in $(CD_3)_2SO$.

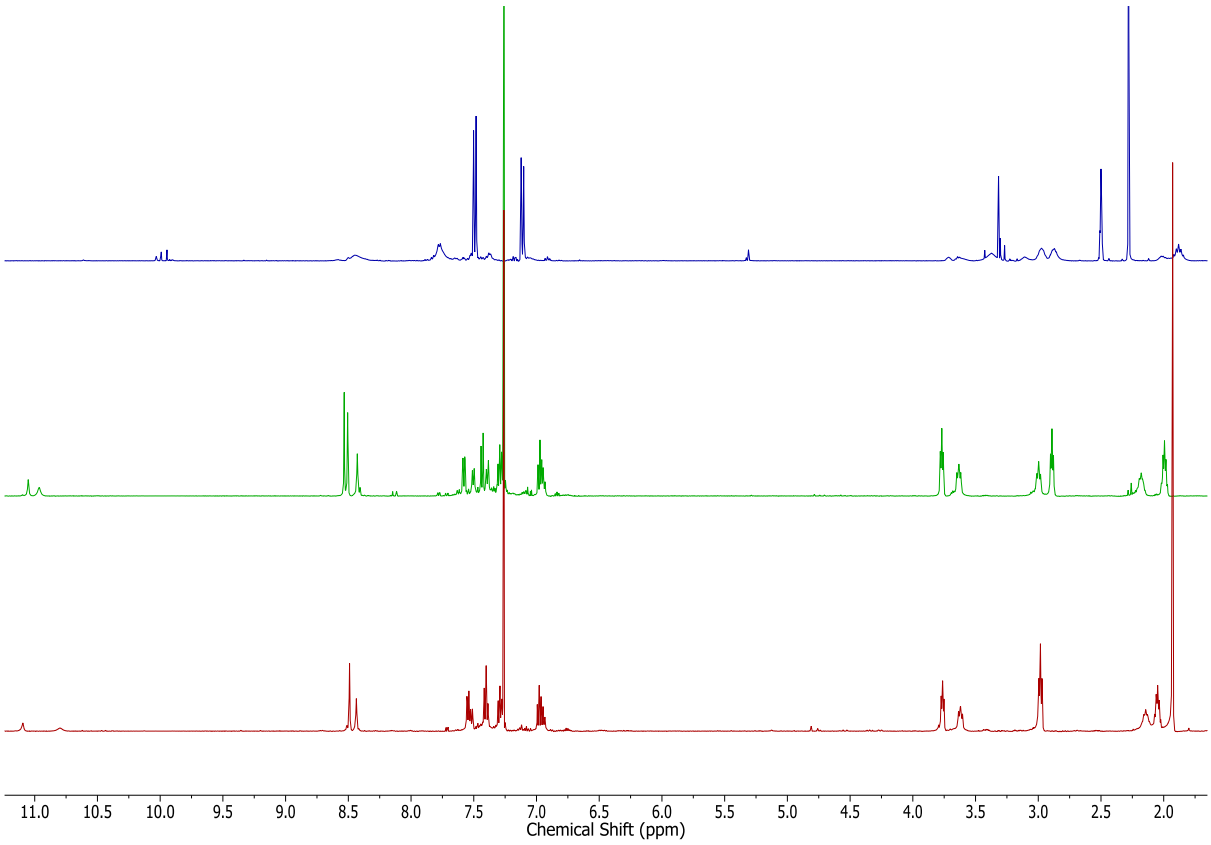

Experimental details for the two 1:1:1 reactions of dialdehyde, diamine and acid which did not work very well.

HL^{Pr}•1.5HOAc•0.5dialdehyde: To a bright yellow solution of **5a** (201 mg, 0.892 mmol) in MeOH (20 mL) was added a solution of dipropylene triamine (117.1 mg, 0.892 mmol) in MeOH (1 mL) resulting in no colour change. A solution of acetic acid (53.6 mg, 0.892 mmol) was added in MeOH (1 mL) resulting in no colour change. The resulting solution was stirred for 48 hours. Solvent was removed under reduced pressure resulting in a bright orange crystalline solid (369 mg, 79%). (Found: C, 68.27; H, 6.85; N, 12.06%. Calc. for [$C_{20}H_{24}N_4$•1.5HOAc•0.5dialdehyde] (523.14 g mol^{-1}): C, 68.62; H, 6.93; N 12.31%).

HL^{Pr}•1.2HCO_2H•0.3dialdehyde: To a bright yellow solution of **5a** (79.4 mg, 0.353 mmol) in MeOH (20 mL) was added a solution of dipropylene triamine (46.3 mg, 0.353 mmol) in MeOH (1 mL) resulting in no colour change. A solution of formic acid (16.2 mg, 0.353 mmol) was added in MeOH (1 mL) resulting in no colour change. The resulting solution was stirred for 48 hours. Solvent was removed under reduced pressure resulting in a bright orange crystalline solid (145 mg, 93%). (Found: C, 69.22; H, 7.10; N, 13.65%. Calc. for [$C_{20}H_{24}N_4$•1.2HCO_2H•0.3dialdehyde] (443.24 g mol^{-1}): C, 68.83; H, 6.75; N 13.59%).

Figure S17. Infrared spectra of all the HL^{Pr} macrocycles, from bottom to top, crude macrocycle HL^{Pr} (green line), HL^{Pr}•2HOAc (purple line), HL^{Pr}•2HCO_2H (red line) and HL^{Pr}•$C_7H_8SO_3$ (blue line).

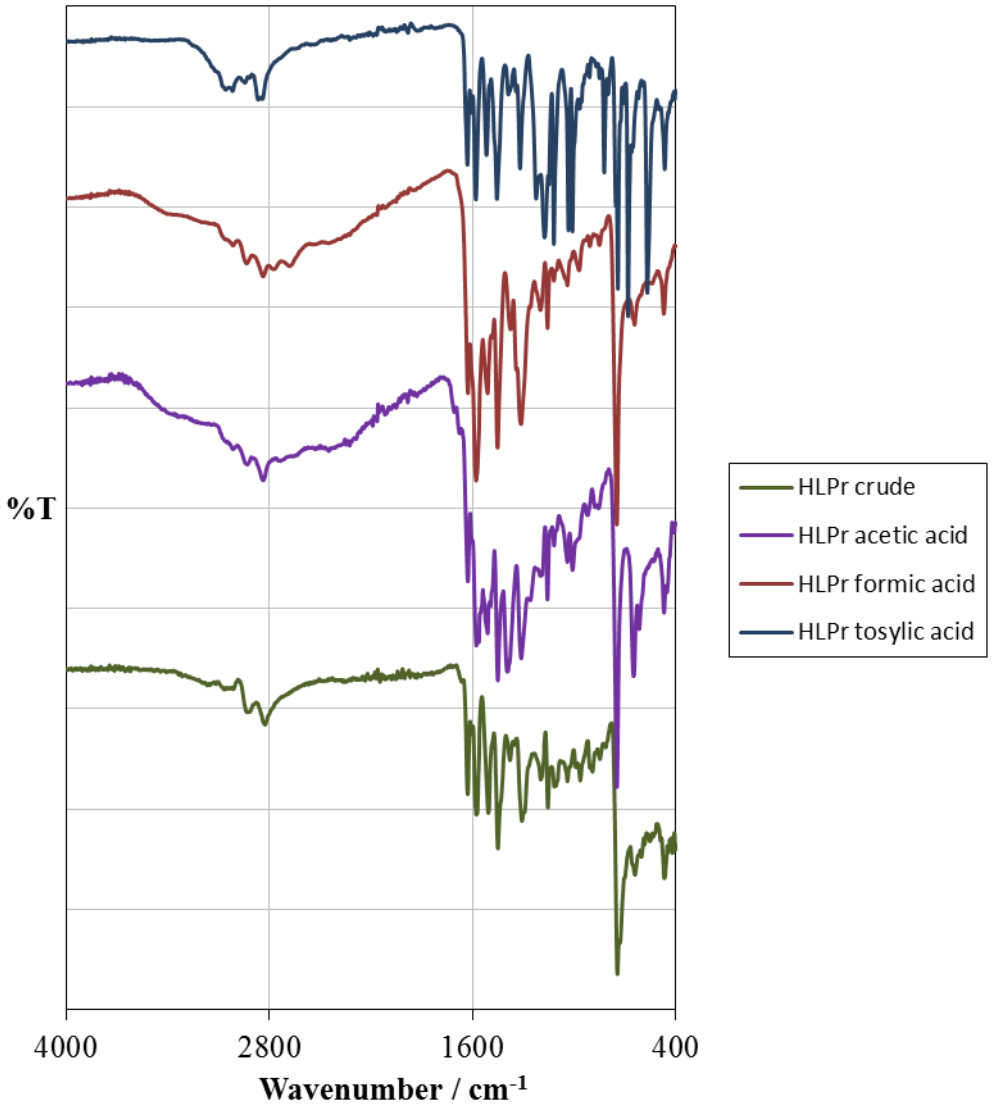

Figure S18. Infrared spectra (expansion of the region between 400-2000 cm^{-1}) of all the HL^{Pr} macrocycles, from bottom to top, crude macrocycle HL^{Pr} (green line), HL^{Pr}•2HOAc (purple line), HL^{Pr}•$2HCO_2H$ (red line) and HL^{Pr}•$C_7H_8SO_3$ (blue line).

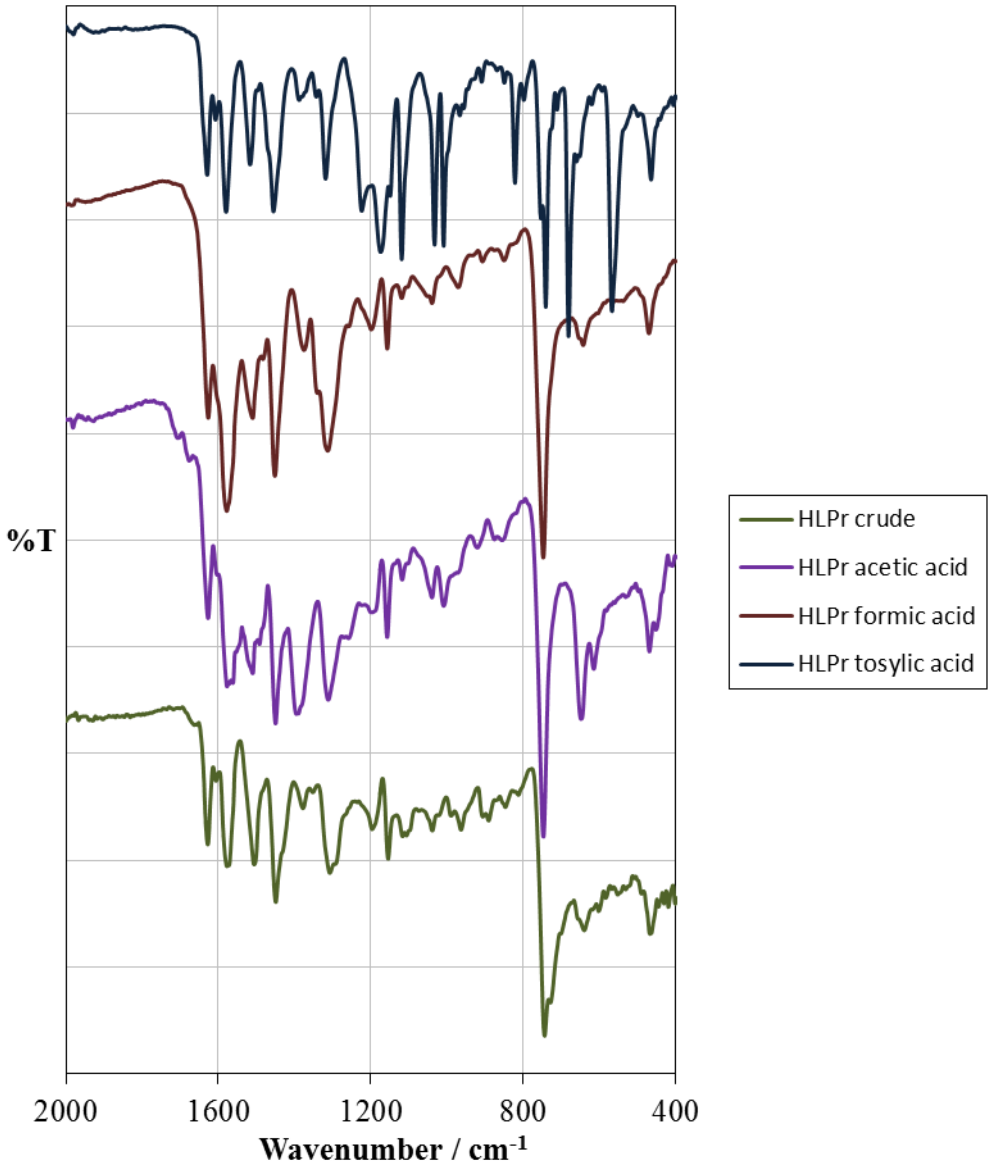

Table S4. Fitting of microanalytical data for the dark red solid obtained by the reaction of crude H**L**^{Pr} with 1 equivalent of $Fe(BF_4)_2 \cdot 6H_2O$ and triethylamine in a 1:1 mixture of DCM and MeCN in air.

	%C	%H	%N
Found	35.56	5.49	6.49
$C_{20}H_{23}N_4FeB_2F_8$	43.57	4.22	10.21
$C_{20}H_{23}N_4FeB_2F_8 \cdot 2.5DCM$	35.50	3.71	7.36

Figure S19. Infrared spectra of the dark red solid obtained by the reaction of crude H**L**^{Pr} with 1 equivalent of $Fe(BF_4)_2 \cdot 6H_2O$ and triethylamine in a 1:1 mixture of DCM and MeCN in air.

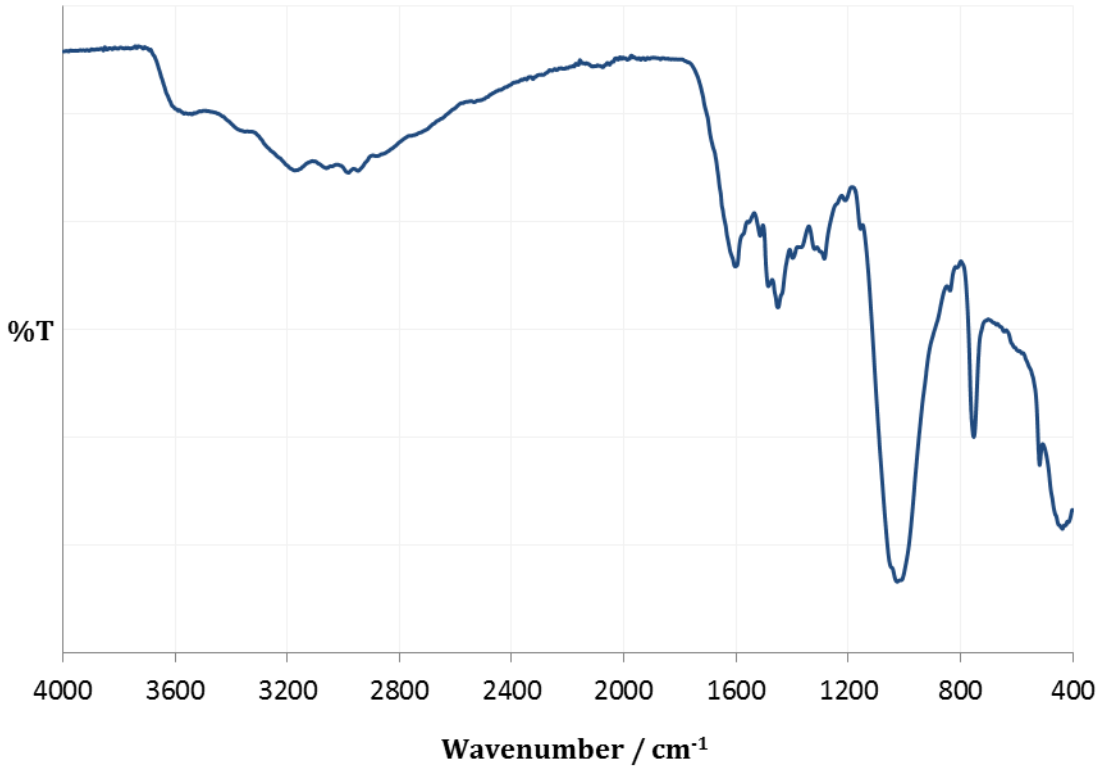

Table S5. Fitting of microanalytical data for the dark red solid obtained by the reaction of crude H**L**^{Pr} with 1 equivalent of $Fe(BF_4)_2 \cdot 6H_2O$ and triethylamine in a 1:1 mixture of DCM and MeCN conducted under an Ar atmosphere, then exposed to air overnight, and then placed in an ether jar for vapour diffusion in air.

	%C	%H	%N
Found	45.43	5.23	10.34
$C_{20}H_{23}N_4FeB_2F_8$	43.57	4.22	10.21
$C_{20}H_{23}N_4FeB_2F_8 \cdot 1.5MeCN$	45.25	4.54	12.62

Figure S20. Infrared spectra of the dark red solid obtained by the reaction of crude H**L**^{Pr} with 1 equivalent of $Fe(BF_4)_2 \cdot 6H_2O$ and triethylamine in a 1:1 mixture of DCM and MeCN under an Ar atmosphere.

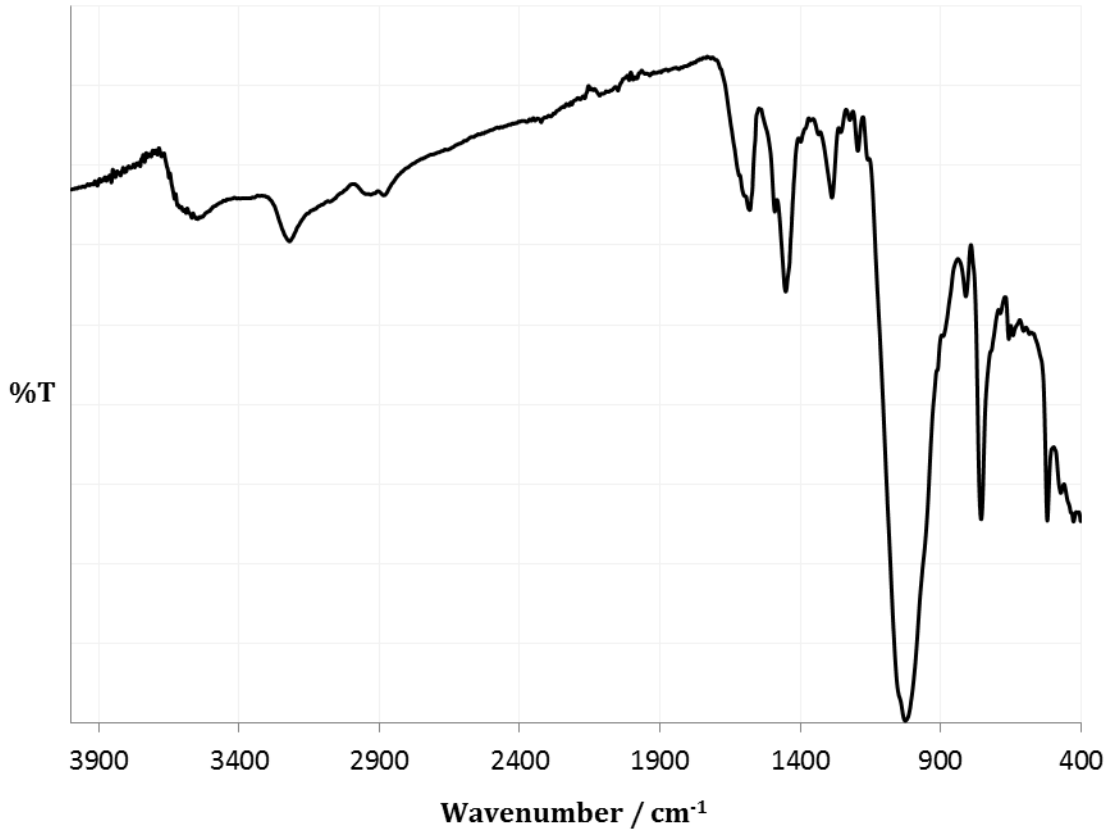

Figure S21. ^{1}H NMR and ^{13}C NMR spectra of $[Ni^{II}L^{Pr}](BF_4)$ in CD_3CN.

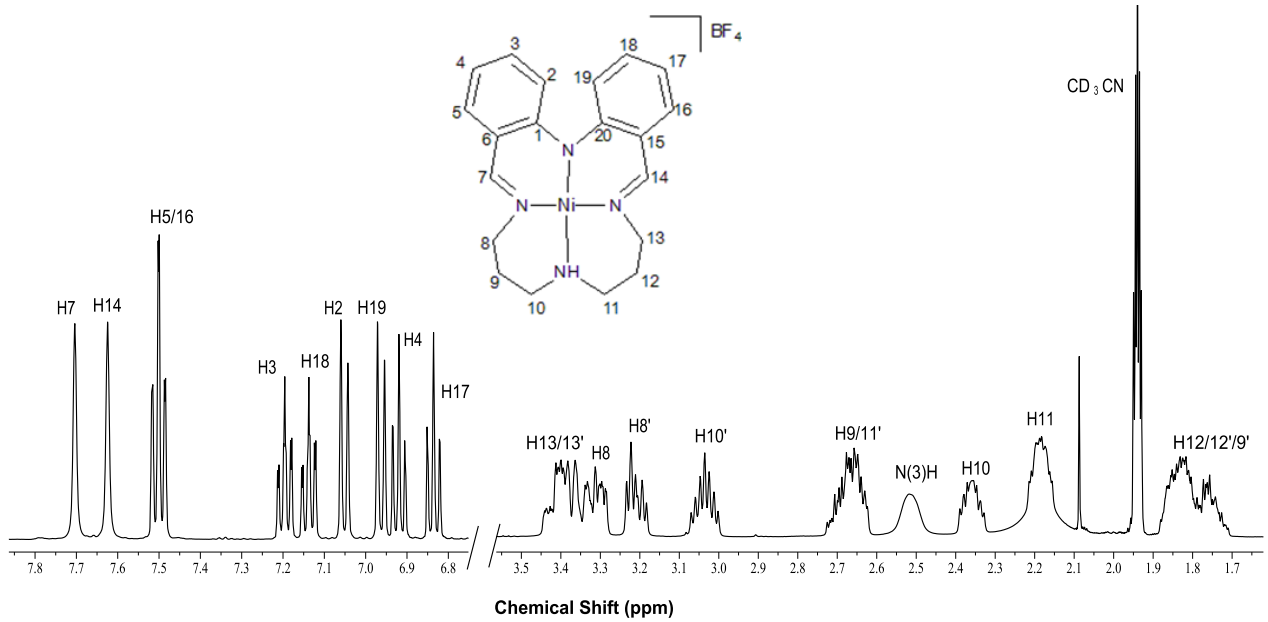

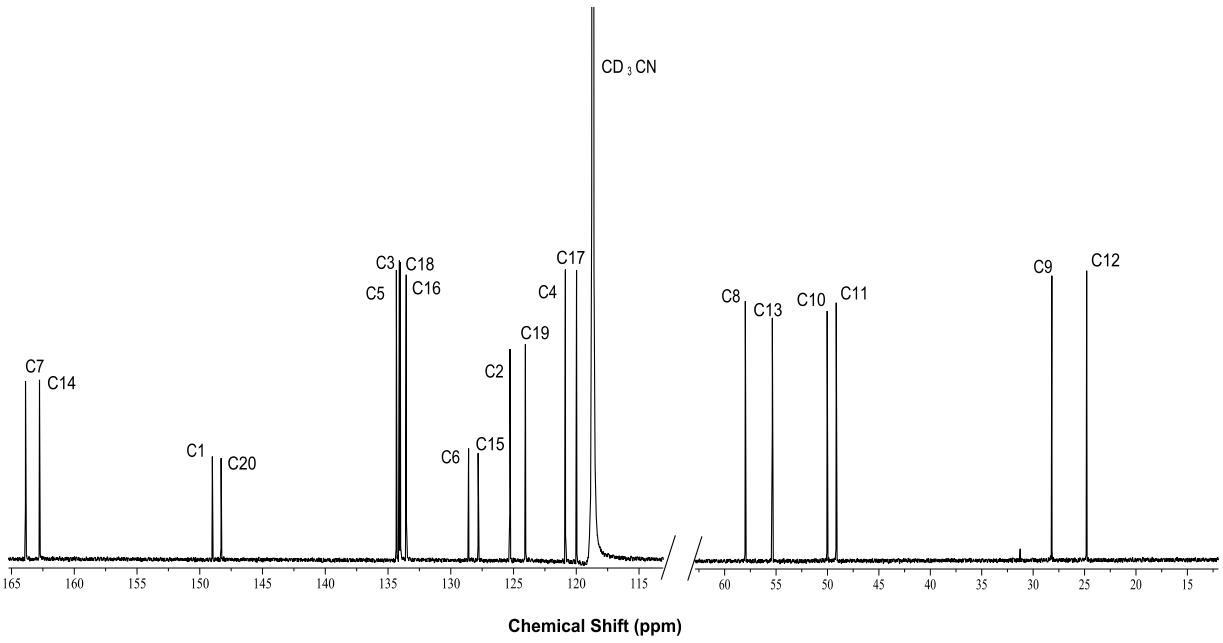

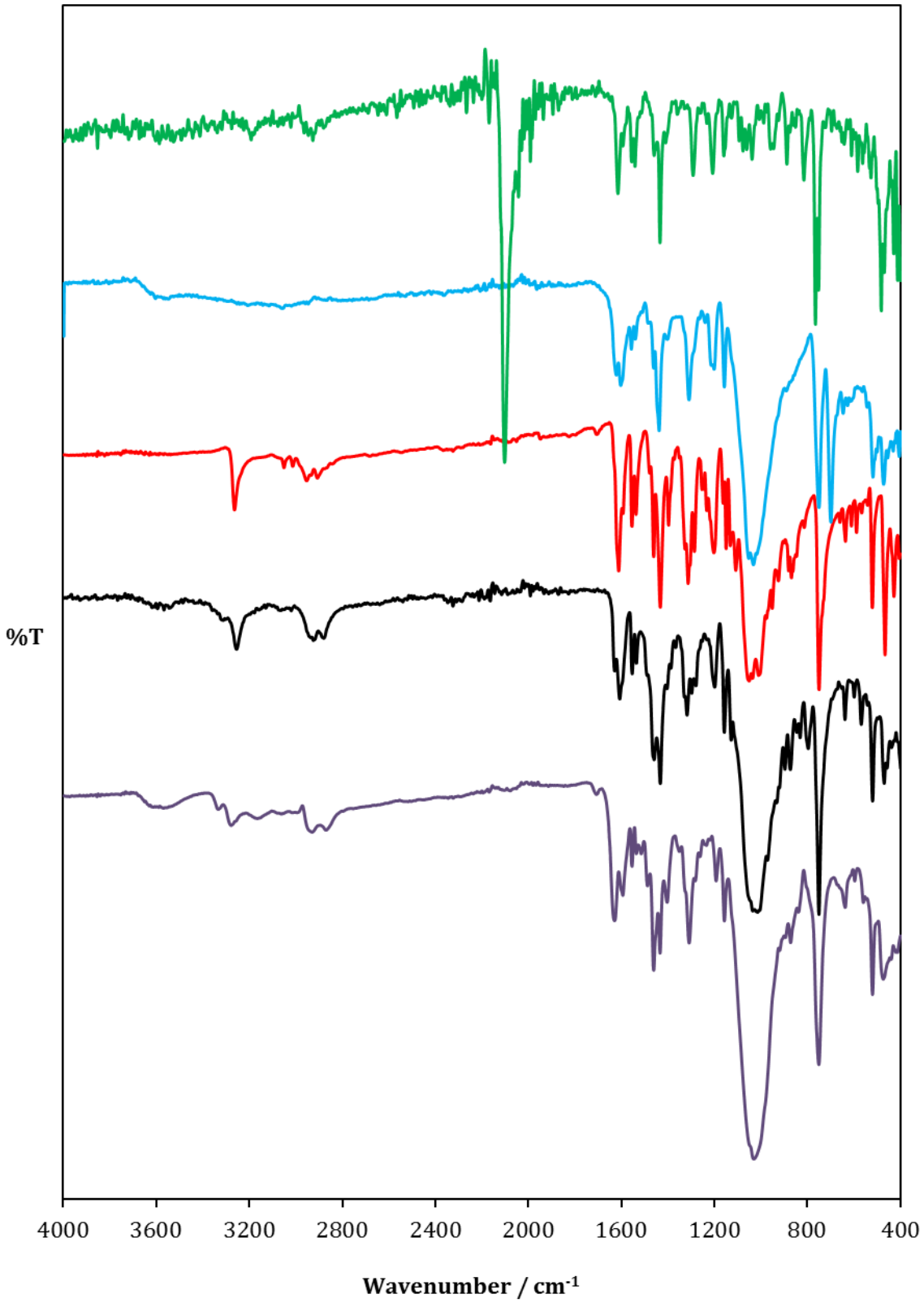

Figure S22. Infrared spectra (ATR) from bottom to top: $Zn^{II}L^{Pr}(BF_4)\bullet 1H_2O\bullet 0.5IPA$ (grey line), $[Cu^{II}L^{Pr}](BF_4)$ (black line), $[Ni^{II}L^{Pr}](BF_4)$ (red line), $[Co^{II}L^{Pr}](BF_4)\bullet 0.5H_2O$ (blue line) and $[Fe^{III}L^{Pr}(NCS)_2]\bullet 1.5H_2O$ (green line).

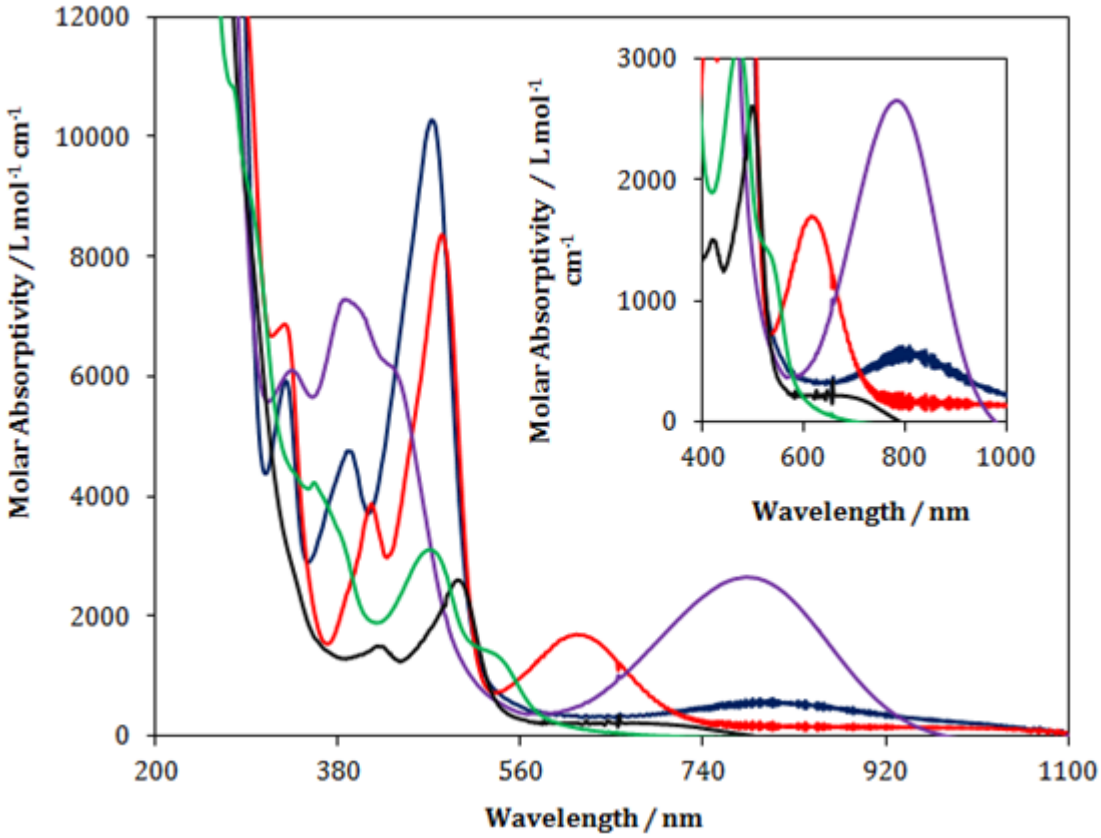

Figure S23. UV-Vis Spectra in CH_3CN at 0.1 mmol L^{-1} for $Zn^{II}L^{Pr}(BF_4)\bullet H_2O\bullet 0.5IPA$ (green line), $[Cu^{II}L^{Pr}](BF_4)$ (blue line), $[Ni^{II}L^{Pr}](BF_4)$ (red line), $[Co^{II}L^{Pr}](BF_4)\bullet 0.5H_2O$ (black line) and $[Fe^{III}L^{Pr}(NCS)_2]\bullet 1.5H_2O$ (purple line). Insert: expansion of the 400-1000 nm region.

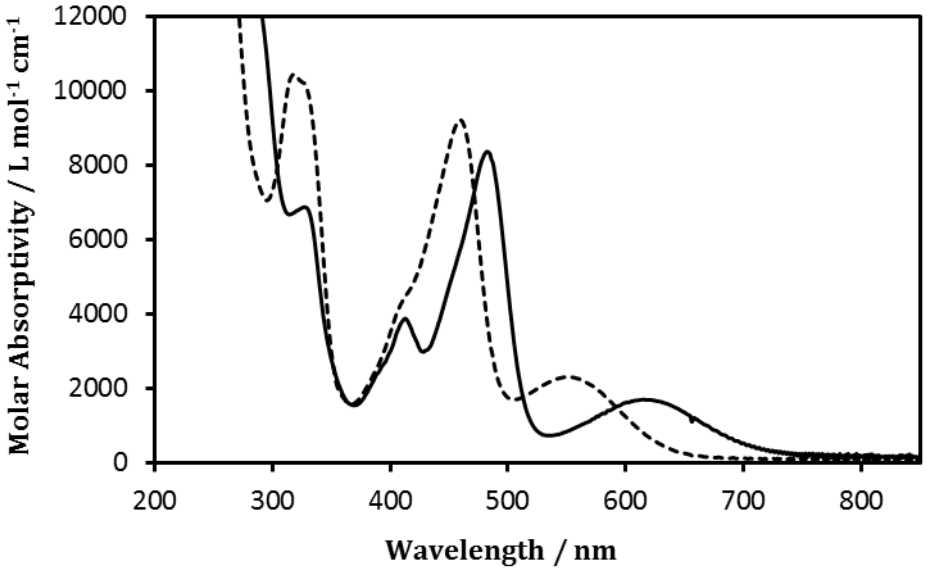

Figure S24. UV-Vis spectra of complexes in CH_3CN at 0.1 mmol L^{-1}: $[Ni^{II}\mathbf{L}^{\mathbf{Pr}}](BF_4)$ (solid line) and $[Ni^{II}\mathbf{L}^{\mathbf{Et}}](BF_4)\bullet H_2O$ (dashed line).

Electrochemical study of $Zn^{II}L^{Pr}(BF_4)•1H_2O•0.5IPA$ in MeCN

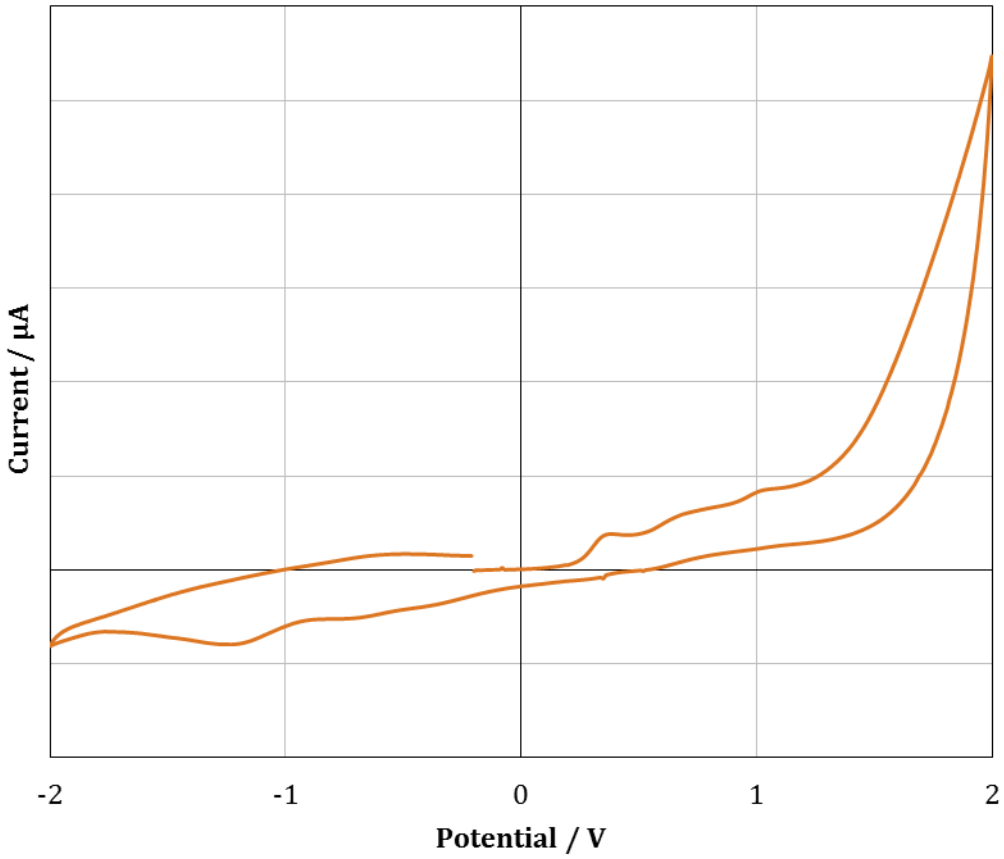

Figure S25. Cyclic voltammogram of $Zn^{II}L^{Pr}(BF_4)•1H_2O•0.5IPA$ as 1 mmol L^{-1} solutions in MeCN (100 mV s^{-1}, 0.1 mol L^{-1} NEt_4PF_6, platinum electrode, versus 0.01 mol L^{-1} $AgNO_3$/Ag).

No controlled coulometry experiment was carried on this complex.

Electrochemical study of $[Cu^{II}L^{Pr}](BF_4)$ in MeCN

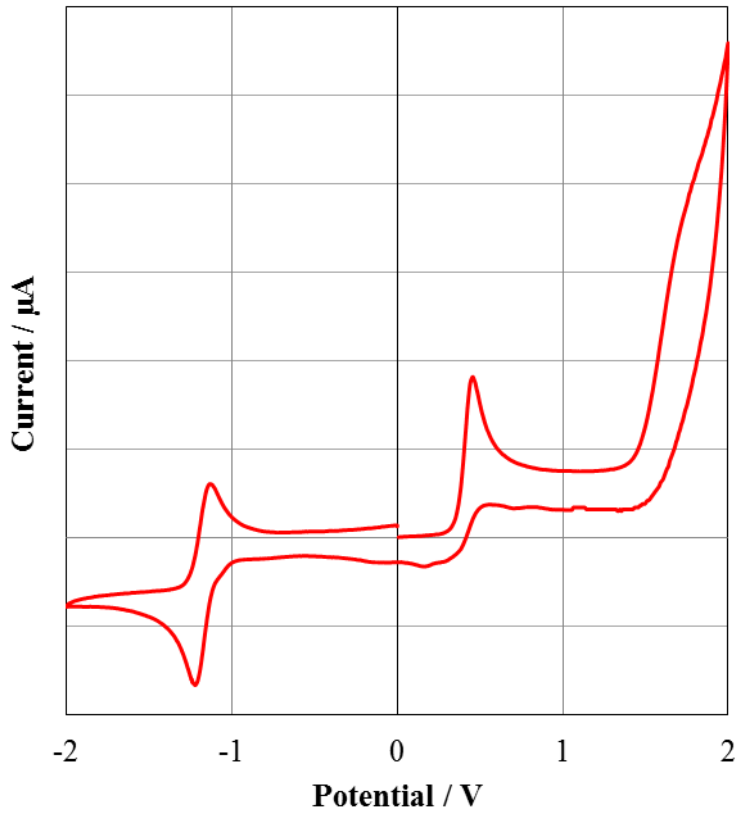

Figure S26. Cyclic voltammogram of $[Cu^{II}L^{Pr}](BF_4)$ before carrying out a controlled potential coulometry experiment at +0.57 V as 1 mmol L^{-1} solutions in MeCN (100 mV s^{-1}, 0.1 mol L^{-1} NEt_4PF_6, platinum electrode, versus 0.01 mol L^{-1} $AgNO_3$/Ag).

Mass of $[Cu^{II}L^{Pr}](BF_4)$ used = 4.6982 mg

Concentration of $[Cu^{II}L^{Pr}](BF_4)$ = (0.0046982) / (0.010 x 469.78) =1.000 x 10^{-3} mol L^{-1}

The expected number of electrons to be transferred provided that this particular process was a one electron process was calculated to be0.97 coulombs. This was calculated from the following equation.

No. of moles of $[Cu^{II}L^{Pr}](BF_4)$ = Concentration of $[Cu^{II}L^{Pr}](BF_4)$ x Volume
= 0.00100 Mol L^{-1} x 0.010 L
= 0.00001 mol

No of electrons transferred = n_e x No. of moles of $[Cu^{II}L^{Pr}](BF_4)$ x Faraday's constant
= 1 x 0.00001 mol x 96500 C mol^{-1}
= 0.965 C if one electron proocess

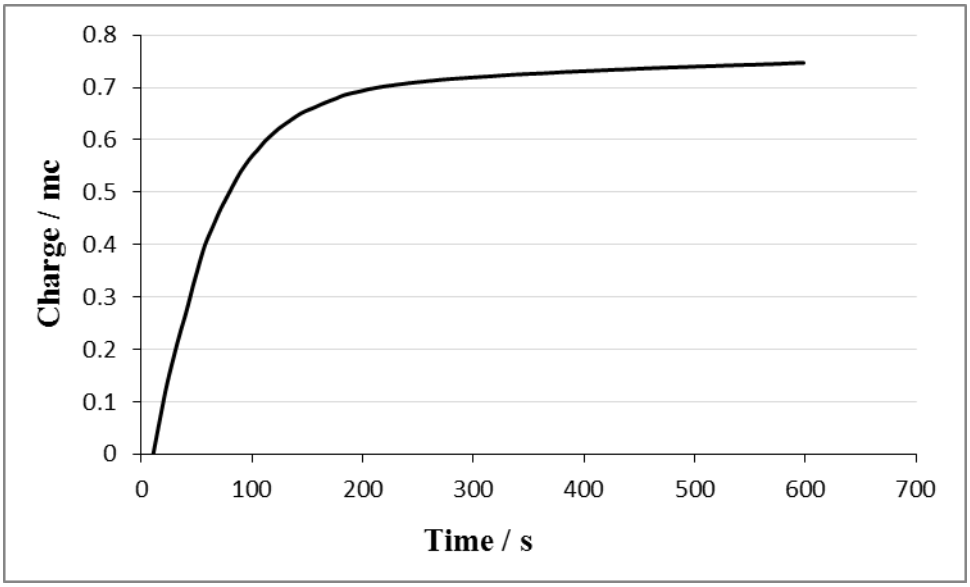

Figure S27. Controlled potentiostatic coulometry experiment conducted at +0.57 V led to 0.78 coulombs of electrons transferred which corresponds to 0.81 electron equivalents per complex.

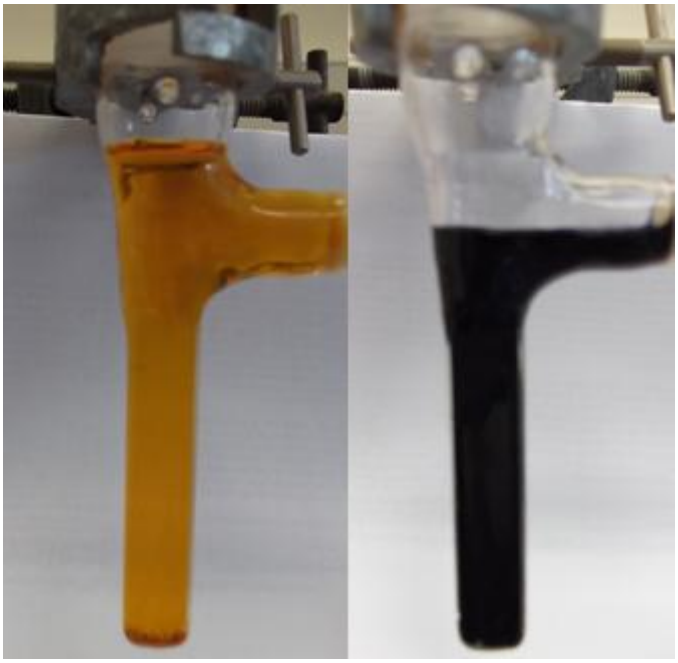

Figure S28. A significant colour change is observed upon controlled potential coulometry experiment at +0.57 V for $[Cu^{II}L^{Pr}](BF_4)$ which resulted in the tansfer (addition) of 0.78 electron equivalents. Left: before; Right: after.

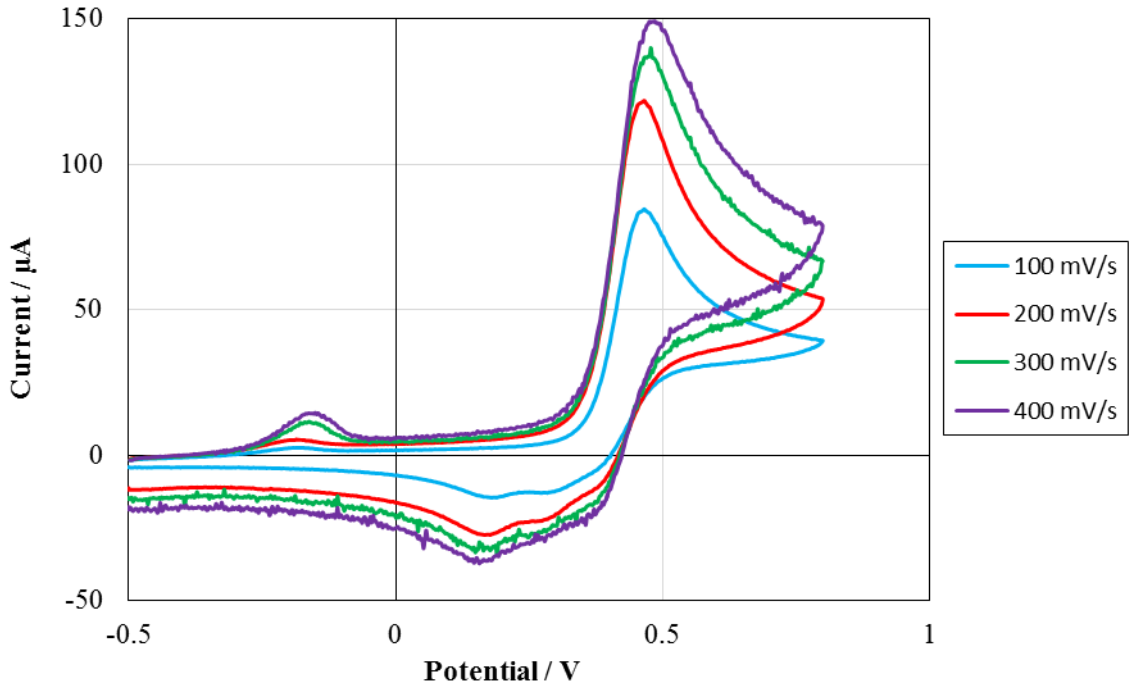

Figure S29. Cyclic voltammogram of $[Cu^{II}L^{Pr}](BF_4)$ (oxidation process) at different scan rates (mV s^{-1}) **before** conducting a controlled coulometry experiment.

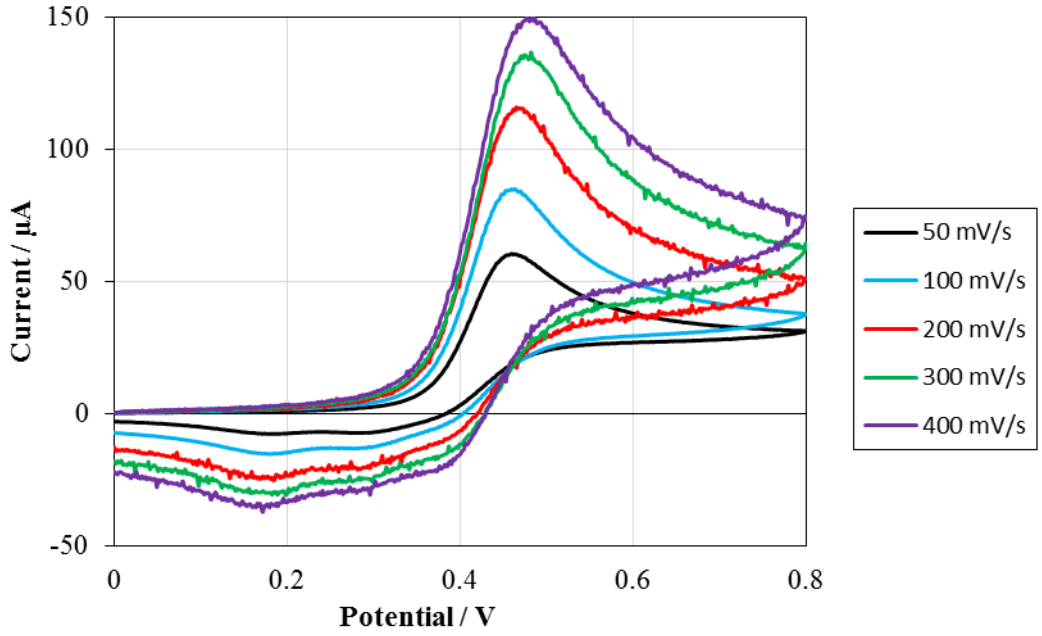

Figure S30. Cyclic voltammogram of $[Cu^{II}L^{Pr}](BF_4)$ (oxidation process) at different scan rates (mV s^{-1}) **before** conducting a controlled coulometry experiment.

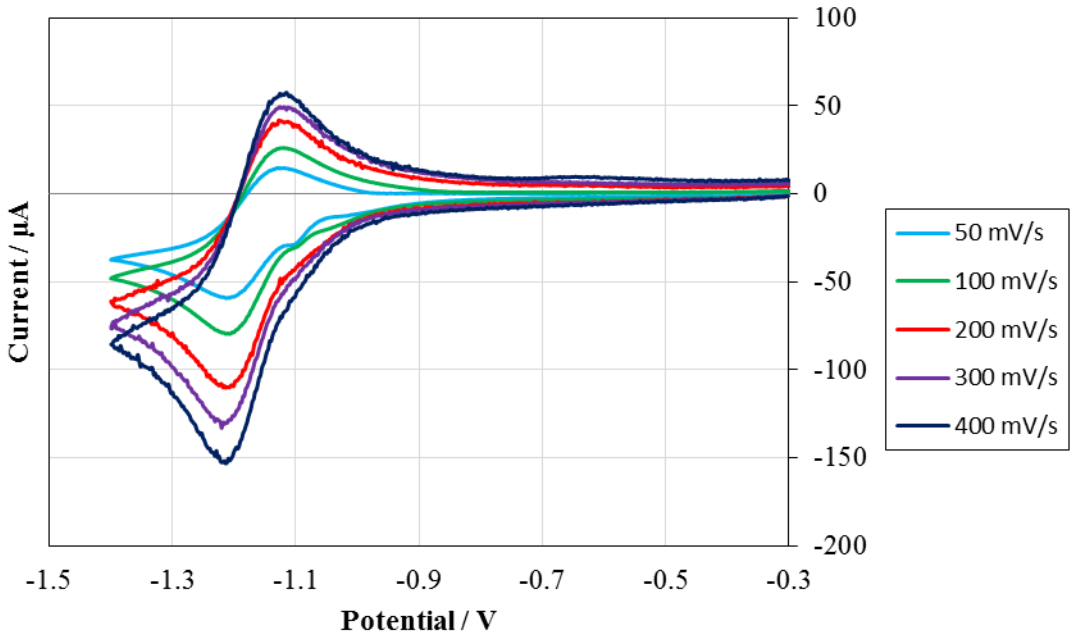

Figure S31. Cyclic voltammogram of $[Cu^{II}L^{Pr}](BF_4)$ (reduction process) at different scan rates (mV s^{-1}) **before** conducting a controlled coulometry experiment.

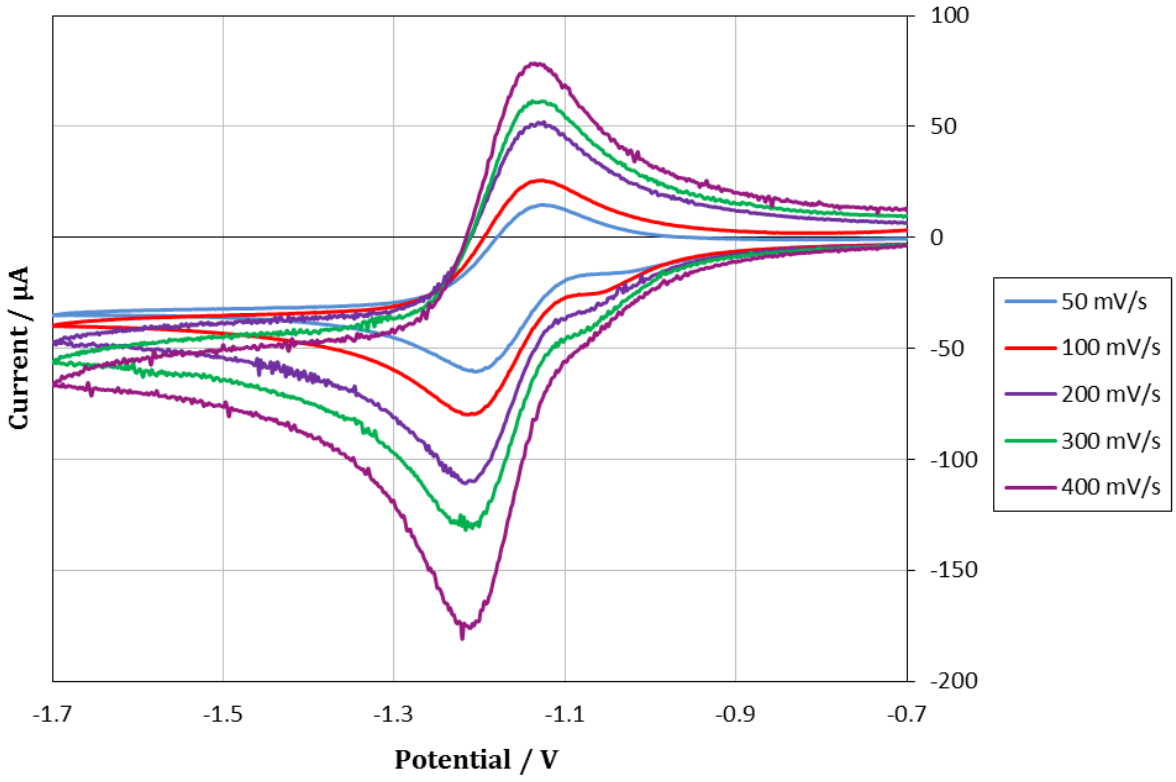

Figure S32. Cyclic voltammogram of $[Cu^{II}L^{Pr}](BF_4)$ (reduction process) at different scan rates (mV s^{-1}) **before** conducting a controlled coulometry experiment.

Table S6. Scan rate study of the process at approximately +0.45 V for $[Cu^{II}L^{Pr}](BF_4)$, from 0 to 0.8 to 0 V (Figure S22), before conducting a controlled coulometry experiment.

Scan Speed / mV S^{-1}	E_{pc}	E_{pa}	ΔE
50	0.45	0.38	0.07
100	0.45	0.39	0.06
200	0.46	0.40	0.06
300	0.47	0.40	0.07
400	0.47	0.39	0.08

Table S7. Scan rate study of the process at approximately -1.20 V for $[Cu^{II}L^{Pr}](BF_4)$ -0.3 to -1.4 to -0.3 (Figure S23), before conducting a controlled coulometry experiment.

Scan Speed / mV S^{-1}	E_{pa}	E_{pc}	ΔE
50	-1.20	-1.14	0.06
100	-1.20	-1.13	0.07
200	-1.20	-1.13	0.07
300	-1.21	-1.13	0.08
400	-1.21	-1.13	0.08

Table S8. Scan rate study of the process at approximately -1.20 V for $[Cu^{II}L^{Pr}](BF_4)$, from -0.7 to -1.7 to -0.7 V (Figure S24), before conducting a controlled coulometry experiment.

Scan Speed / mV S^{-1}	E_{pa}	E_{pc}	ΔE
50	-1.19	-1.14	0.05
100	-1.20	-1.14	0.06
200	-1.20	-1.14	0.06
300	-1.21	-1.14	0.07
400	-1.21	-1.15	0.06

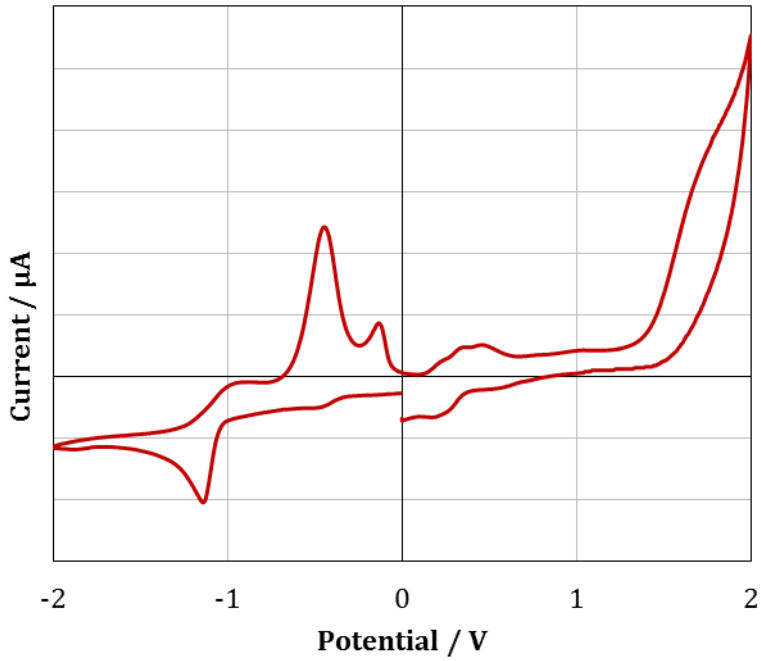

Figure S33. Cyclic voltammogram of $[Cu^{II}L^{Pr}](BF_4)$ **after** carrying out a controlled potential coulometry experiment at +0.57 as 1 mmol L^{-1} solutions in MeCN (100 mV s^{-1}, 0.1 mol L^{-1} NEt_4PF_6, platinum electrode, versus 0.01 mol L^{-1} $AgNO_3$/Ag).

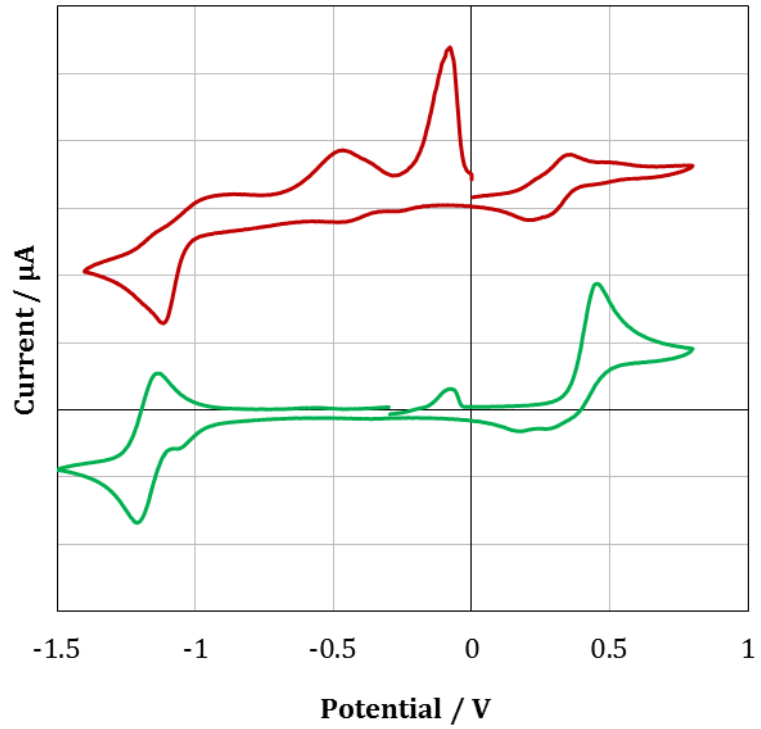

Figure S34. Cyclic voltammogram, from the bottom of $[Cu^{II}L^{Pr}](BF_4)$ **before** (green) and **after** (red) carrying out a controlled potential coulometry experiment at +0.57 as 1 mmol L^{-1} solutions in MeCN (100 mV s^{-1}, 0.1 mol L^{-1} NEt_4PF_6, platinum electrode, versus 0.01 mol L^{-1} $AgNO_3$/Ag).

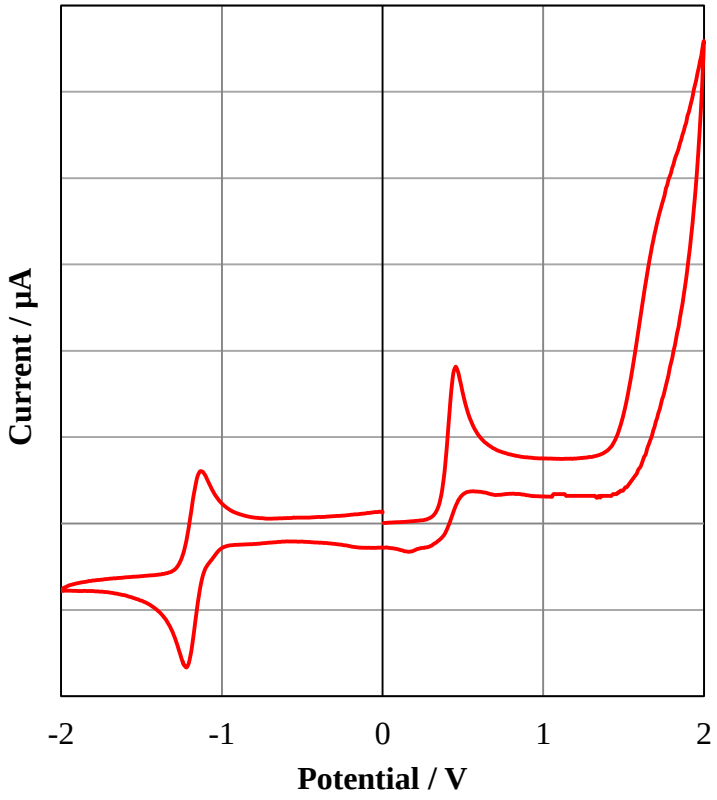

Figure S35. Cyclic voltammogram of $[Cu^{II}L^{Pr}](BF_4)$ before carrying out a controlled potential coulometry experiment at -1.30 V as 1 mmol L^{-1} solutions in MeCN (100 mV s^{-1}, 0.1 mol L^{-1} NEt_4PF_6, platinum electrode, versus 0.01 mol L^{-1} $AgNO_3$/Ag).

1. First bulk electrolysis experiment, at -1.30 V

Mass of $[Cu^{II}L^{Pr}](BF_4)$ used = 4.6972mg

Concentration of $[Cu^{II}L^{Pr}](BF_4)$ = (0.0046972) / (0.010 x 469.78) =9.99 x 10^{-4} mol L^{-1}

The expected number of electrons to be transferred provided that this particular process was a one electron process was calculated to be0.96 coulombs. This was calculated from the following equation.

No. of moles of $[Cu^{II}L^{Pr}](BF_4)$ = Concentration of $[Cu^{II}L^{Pr}](BF_4)$ x Volume
= 0.000999 Mol L^{-1} x 0.010 L
= 0.00000999 mol

No of electrons transferred = n_e x No. of moles of $[Cu^{II}L^{Pr}](BF_4)$ x Faraday's constant
= 1 x 0.00000999 mol x 96500 C mol^{-1}
= 0.964 C if one electron proocess

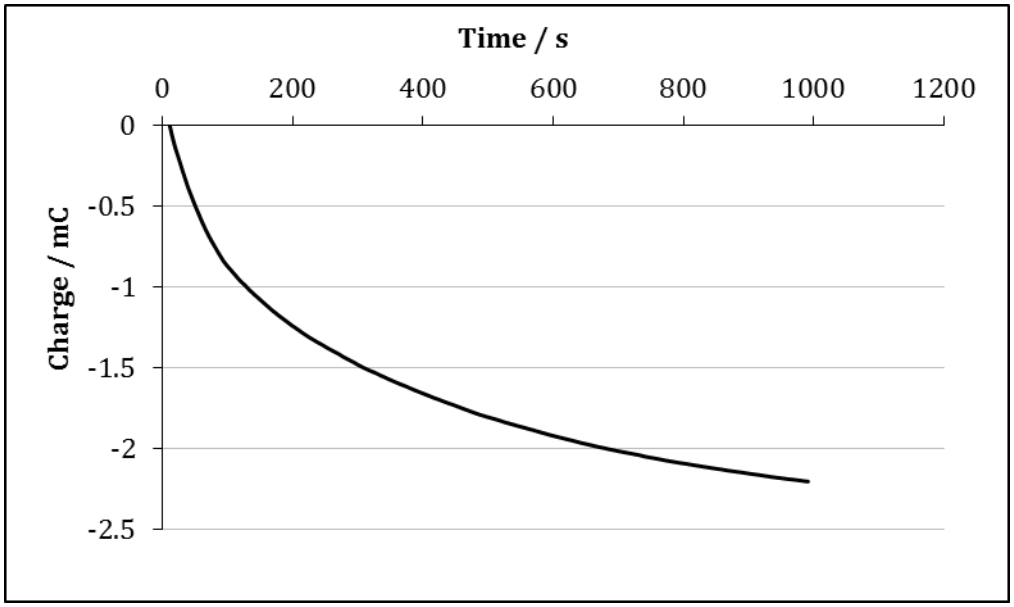

Figure S36. Controlled potentiostatic coulometry experiment conducted at -1.30 V led to 2.20 coulombs of electrons transferred which corresponds to 2.30 electron equivalents per complex.

2. Second bulk electrolysis experiment, at -1.35 V

A controlled potentiostatic coulometry experiment was also carried out, on a fresh sample, at -1.35 V.

Mass of $[Cu^{II}L^{Pr}](BF_4)$ used = 4.6960mg

Concentration of $[Cu^{II}L^{Pr}](BF_4)$ = (0.0046960) / (0.010 x 469.78) =9.99 x 10^{-4} mol L^{-1}

The expected number of electrons to be transferred provided that this particular process was a one electron process was calculated to be0.96 coulombs. This was calculated from the following equation.

No. of moles of $[Cu^{II}L^{Pr}](BF_4)$ = Concentration of $[Cu^{II}L^{Pr}](BF_4)$ x Volume
= 0.000999 Mol L^{-1} x 0.010 L
= 0.00000999 mol

No of electrons transferred = n_e x No. of moles of $[Cu^{II}L^{Pr}](BF_4)$ x Faraday's constant
= 1 x 0.00000999 mol x 96500 C mol^{-1}
= 0.964 C if one electron proocess

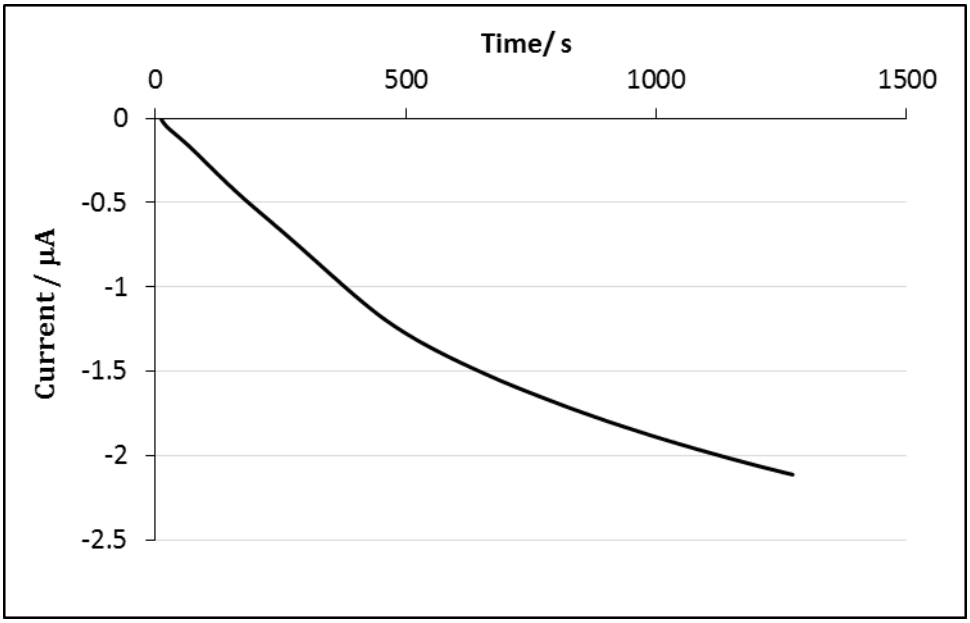

Figure S37. Controlled potentiostatic coulometry experiment conducted at -1.35 V led to 2.10 coulombs of electrons transferred which corresponds to 2.20 electron equivalents per complex.

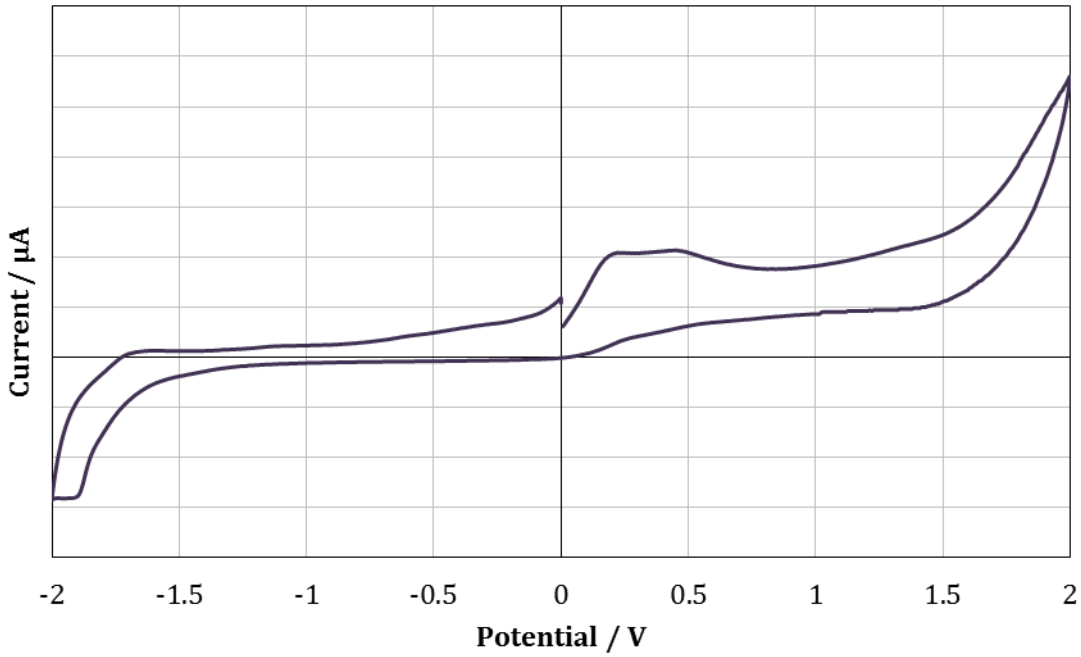

Figure S38. Cyclic voltammogram of $[Cu^{II}L^{Pr}](BF_4)$ **after** carrying out a controlled potential coulometry experiment at -1.30 as 1 mmol L^{-1} solutions in MeCN (100 mV s^{-1}, 0.1 mol L^{-1} NEt_4PF_6, platinum electrode, versus 0.01 mol L^{-1} $AgNO_3$/Ag).

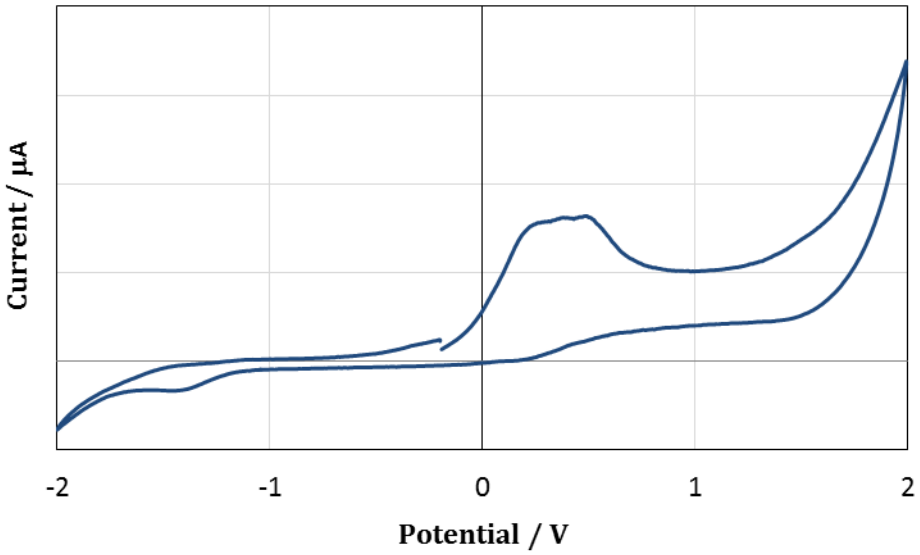

Figure S39. Cyclic voltammogram of $[Cu^{II}L^{Pr}](BF_4)$ **after** carrying out a controlled potential coulometry experiment at -1.35 as 1 mmol L^{-1} solutions in MeCN (100 mV s^{-1}, 0.1 mol L^{-1} NEt_4PF_6, platinum electrode, versus 0.01 mol L^{-1} $AgNO_3$/Ag).

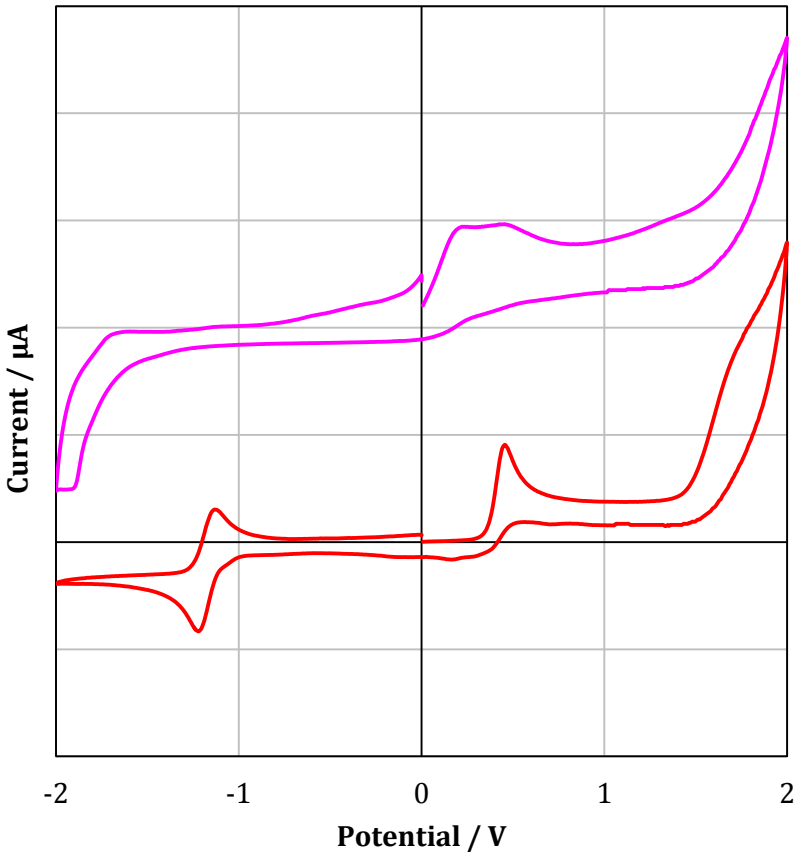

Figure S40. Cyclic voltammogram, from the bottom of $[Cu^{II}L^{Pr}](BF_4)$ **before** (red) and **after** (pink) carrying out a controlled potential coulometry experiment at -1.30 as 1 mmol L^{-1} solutions in MeCN (100 mV s^{-1}, 0.1 mol L^{-1} NEt_4PF_6, platinum electrode, versus 0.01 mol L^{-1} $AgNO_3$/Ag).

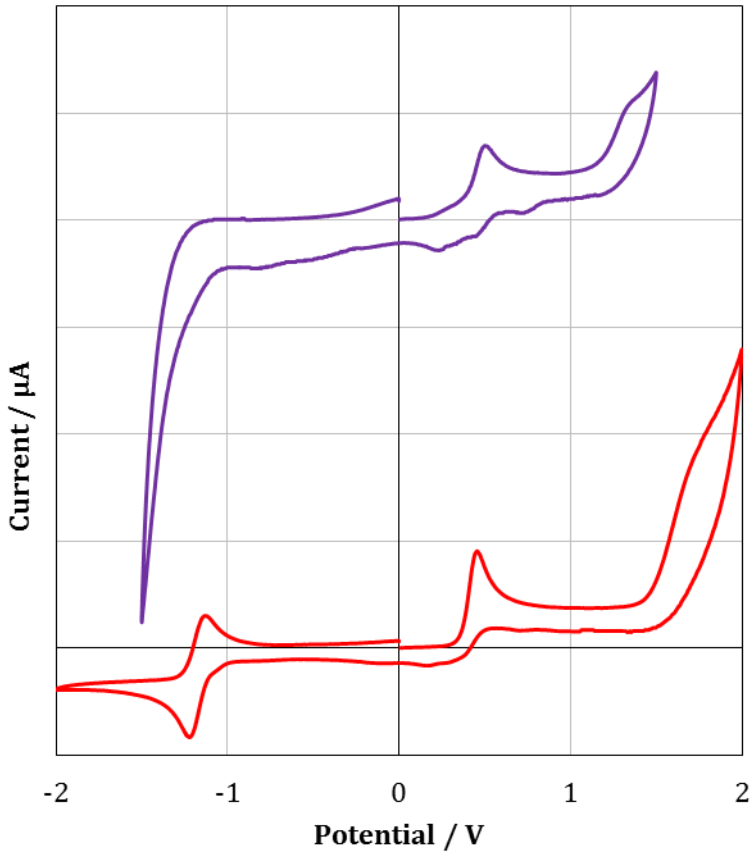

Figure S41. Comparison of the CVs of from bottom to top for $[Cu^{II}L^{Pr}](BF_4)$ (red) and $[Cu^{II}L^{Et}](BF_4)\bullet H_2O$ (purple) before carrying out a controlled potential coulometry experiment as 1 mmol L^{-1} solutions in MeCN (100 mV s^{-1}, 0.1 M NEt_4PF_6, platinum electrode, versus 0.01 M $AgNO_3$/Ag).

Electrochemical study of $[Ni^{II}L^{Pr}](BF_4)$ in MeCN

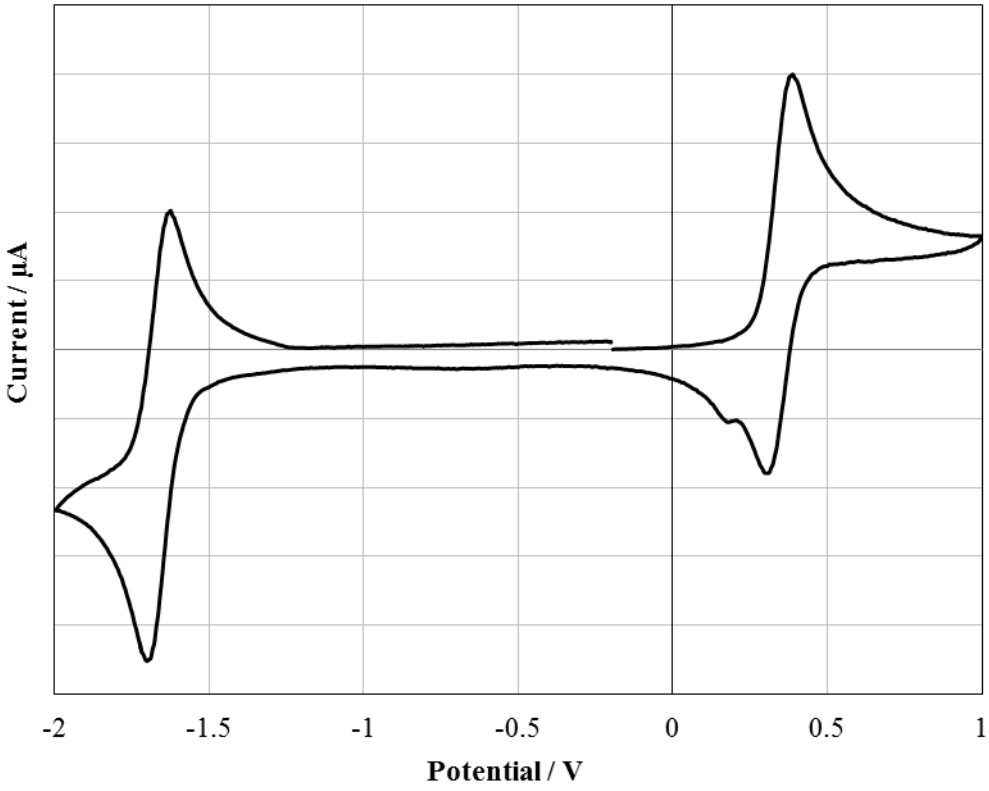

Figure S42. Cyclic voltammogram of $[Ni^{II}L^{Pr}](BF_4)$ **before** carrying out a controlled potential coulometry experiment at +0.51 V as 1 mmol L^{-1} solutions in MeCN (100 mV s^{-1}, 0.1 mol L^{-1} NEt_4PF_6, platinum electrode, versus 0.01 mol L^{-1} $AgNO_3$/Ag).

Mass of $[Ni^{II}L^{Pr}](BF_4)$ used = 4.6657 mg

Concentration of $[Ni^{II}L^{Pr}](BF_4)$ = (0.0046657) / (0.010 x 464.92) =1.000 x 10^{-3} mol L^{-1}

The expected number of electrons to be transferred provided that this particular process was a one electron process was calculated to be0.97 coulombs. This was calculated from the following equation.

No. of moles of $[Ni^{II}L^{Pr}](BF_4)$ = Concentration of $[Ni^{II}L^{Pr}](BF_4)$ x Volume
= 0.00100 Mol L^{-1} x 0.010 L
= 0.00001 mol

No of electrons transferred = n_e x No. of moles of $[Ni^{II}L^{Pr}](BF_4)$ x Faraday's constant
= 1 x 0.00001 mol x 96500 C mol^{-1}
= 0.965 C if one electron proocess

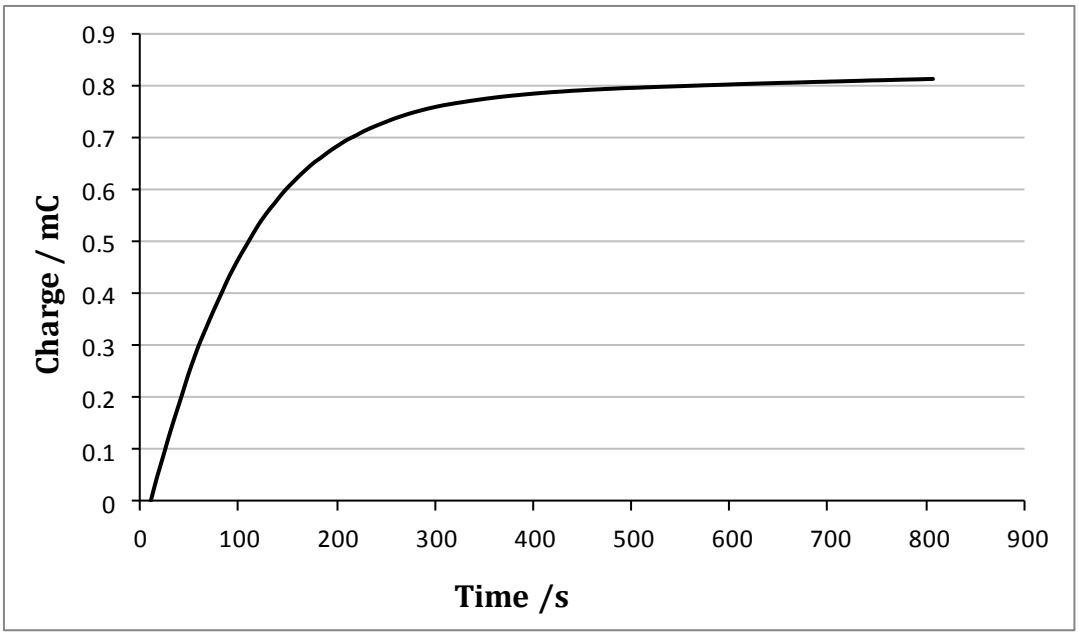

Figure S43. Controlled potentiostatic coulometry experiment conducted at +0.51 V led to 0.81 coulombs of electrons transferred which corresponds to 0.84 electron equivalents per complex.

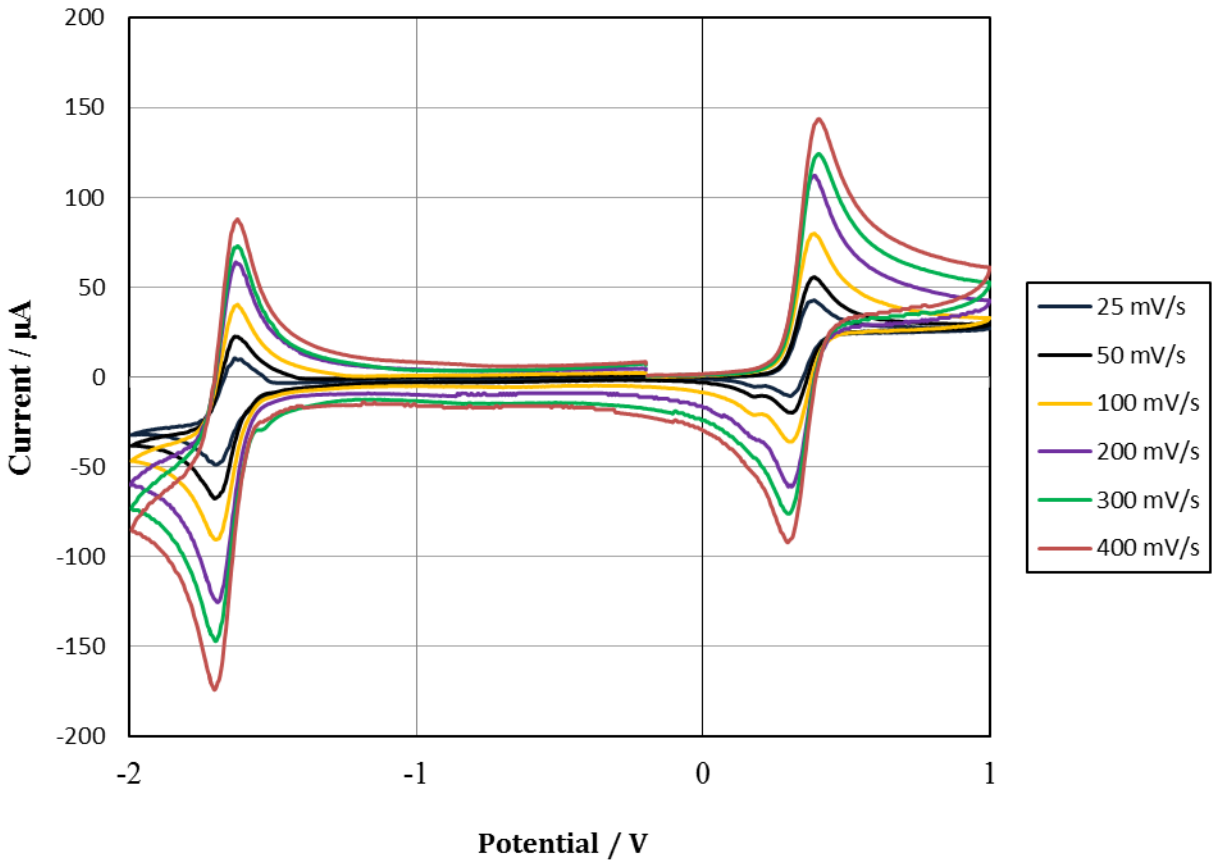

Figure S44. Cyclic voltammogram of $[Ni^{II}L^{Pr}](BF_4)$ (full scan) at different scan rates (mV s^{-1}) **before** conducting a controlled coulometry experiment.

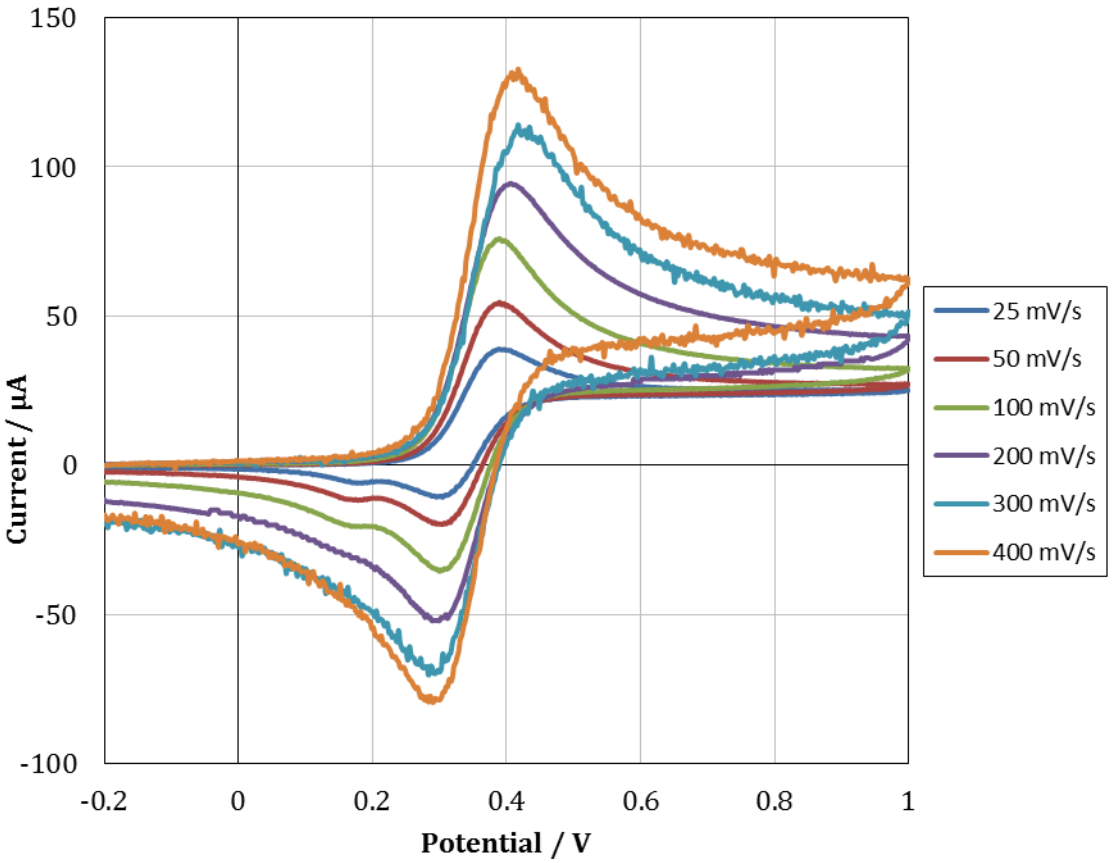

Figure S45. Cyclic voltammogram of $[Ni^{II}L^{Pr}](BF_4)$ (oxidation process) at different scan rates (mV s^{-1}) **before** conducting a controlled coulometry experiment.

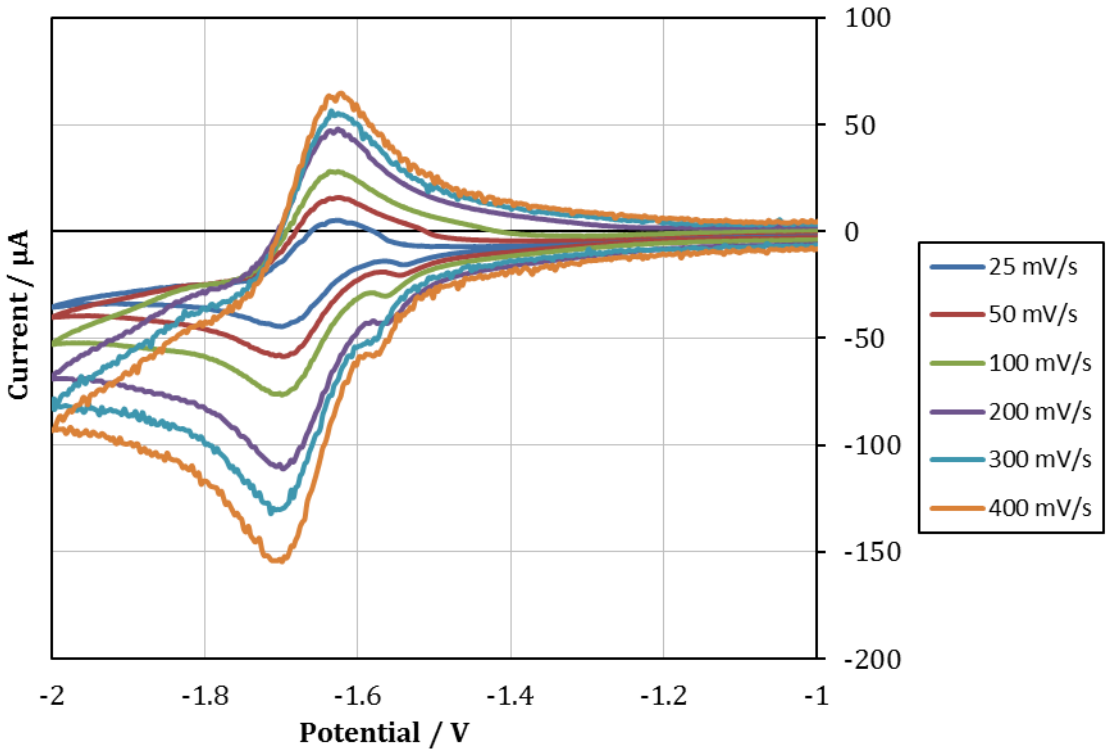

Figure S46. Cyclic voltammogram of $[Ni^{II}L^{Pr}](BF_4)$ (reduction process) at different scan rates (mV s^{-1}) **before** conducting a controlled coulometry experiment.

Table S9. Scan rate study of the process at approximately +0.38 V for $[Ni^{II}L^{Pr}](BF_4)$, from 0 to 1.0 to -2 to 0 V, **before** conducting a controlled coulometry experiment.

Scan Speed / mV S^{-1}	E_{pc}	E_{pa}	ΔE	i_{pa}/i_{pc}	i_{pa}/i_{pc} (Fc/Fc^+)	ΔE (Fc/Fc^+)
25	0.37	0.32	0.05	0.8	1.0	0.06
50	0.38	0.32	0.06	0.8	0.9	0.06
100	0.38	0.32	0.06	0.7	1.0	0.06
200	0.38	0.32	0.06	0.8	0.9	0.07
300	0.39	0.31	0.08	0.8	0.9	0.07
400	0.39	0.31	0.08	0.9	0.9	0.08

Table S10. Scan rate study of the process at approximately -1.69 V for $[Ni^{II}L^{Pr}](BF_4)$, from 0 to 1.0 to -2 to 0 V, **before** conducting a controlled coulometry experiment.

Scan Speed / mV S^{-1}	E_{pa}	E_{pc}	ΔE	i_{pa}/i_{pc}
25	-1.69	-1.64	0.05	1.1
50	-1.69	-1.64	0.05	1.1
100	-1.70	-1.64	0.06	1.2
200	-1.68	-1.65	0.03	1.2
300	-1.69	-1.64	0.05	1.1
400	-1.70	-1.64	0.06	1.3

Table S11. Scan rate study of the process at approximately +0.40 V for $[Ni^{II}L^{Pr}](BF_4)$, from -0.2 to 1.0 to -0.2 V, **before** conducting a controlled coulometry experiment.

Scan Speed / mV S^{-1}	E_{pc}	E_{pa}	ΔE	i_{pa}/i_{pc}
25	0.37	0.32	0.05	0.9
50	0.37	0.32	0.05	0.9
100	0.37	0.32	0.05	0.8
200	0.39	0.31	0.08	0.9
300	0.41	0.31	0.10	0.9
400	0.40	0.30	0.10	0.9

Table S12. Scan rate study of the process at approximately -1.69 V for $[Ni^{II}L^{Pr}](BF_4)$, from -1.0 to -2.0 to -1.0 V, **before** conducting a controlled coulometry experiment.

Scan Speed / mV S^{-1}	E_{pa}	E_{pc}	ΔE	i_{pa}/i_{pc}
25	-1.69	-1.65	0.04	1.1
50	-1.69	-1.65	0.04	1.1
100	-1.69	-1.65	0.04	1.2
200	-1.69	-1.64	0.05	1.2
300	-1.69	-1.64	0.05	1.1
400	-1.69	-1.64	0.05	1.3

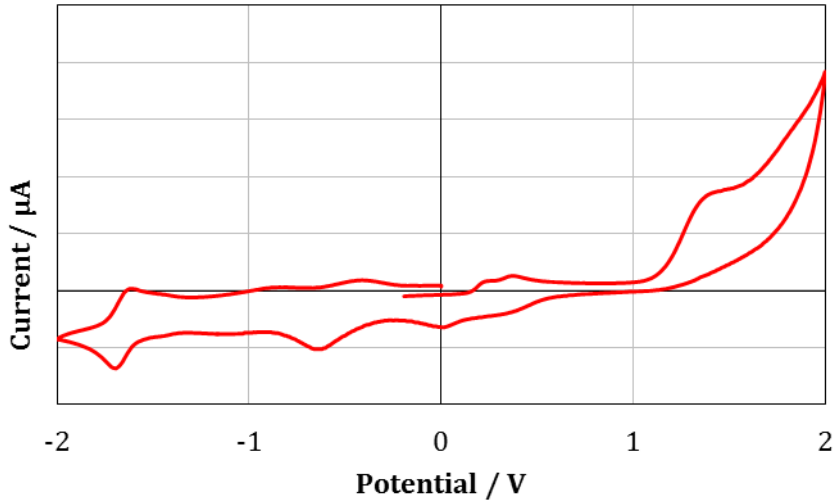

Figure S47. Cyclic voltammogram of $[Ni^{II}L^{Pr}](BF_4)$ **after** carrying out a controlled potential coulometry experiment at +0.51 as 1 mmol L^{-1} solutions in MeCN (200 mV s^{-1}, 0.1 mol L^{-1} NEt_4PF_6, platinum electrode, versus 0.01 mol L^{-1} $AgNO_3$/Ag).

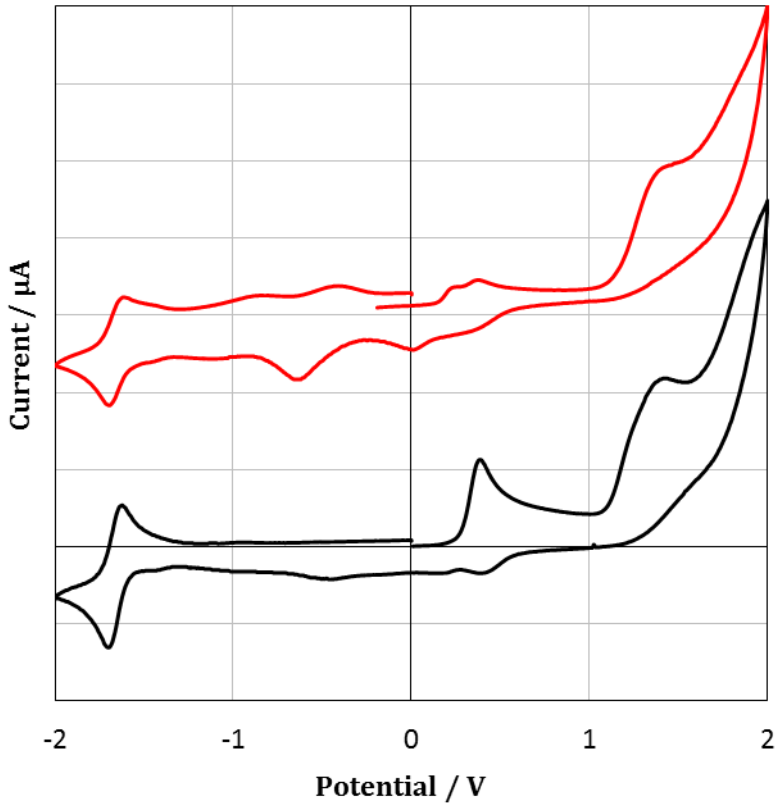

Figure S48. Cyclic voltammogram, from the bottom of $[Ni^{II}L^{Pr}](BF_4)$ **before** (purple) and **after** (blue) carrying out a controlled potential coulometry experiment at +0.51 as 1 mmol L^{-1} solutions in MeCN (200 mV s^{-1}, 0.1 mol L^{-1} NEt_4PF_6, platinum electrode, versus 0.01 mol L^{-1} $AgNO_3$/Ag).

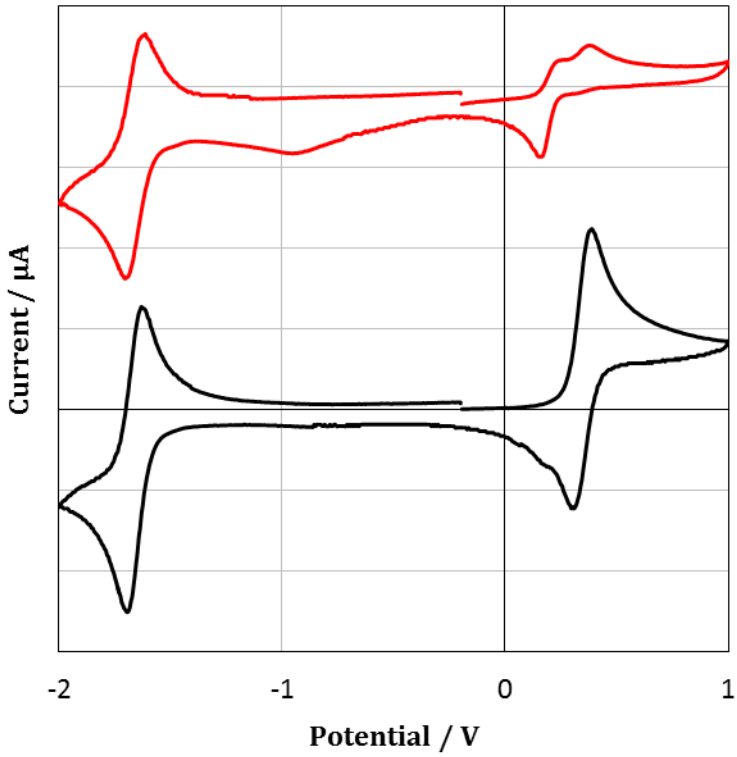

Figure S49. Cyclic voltammogram from the bottom $[Ni^{II}L^{Pr}](BF_4)$ **before** (purple) and **after** (blue) carrying out a controlled potential coulometry experiment at +0.51 as 1 mmol L^{-1} solutions in MeCN (200 mV s^{-1}, 0.1 mol L^{-1} NEt_4PF_6, platinum electrode, versus 0.01 mol L^{-1} $AgNO_3$/Ag).

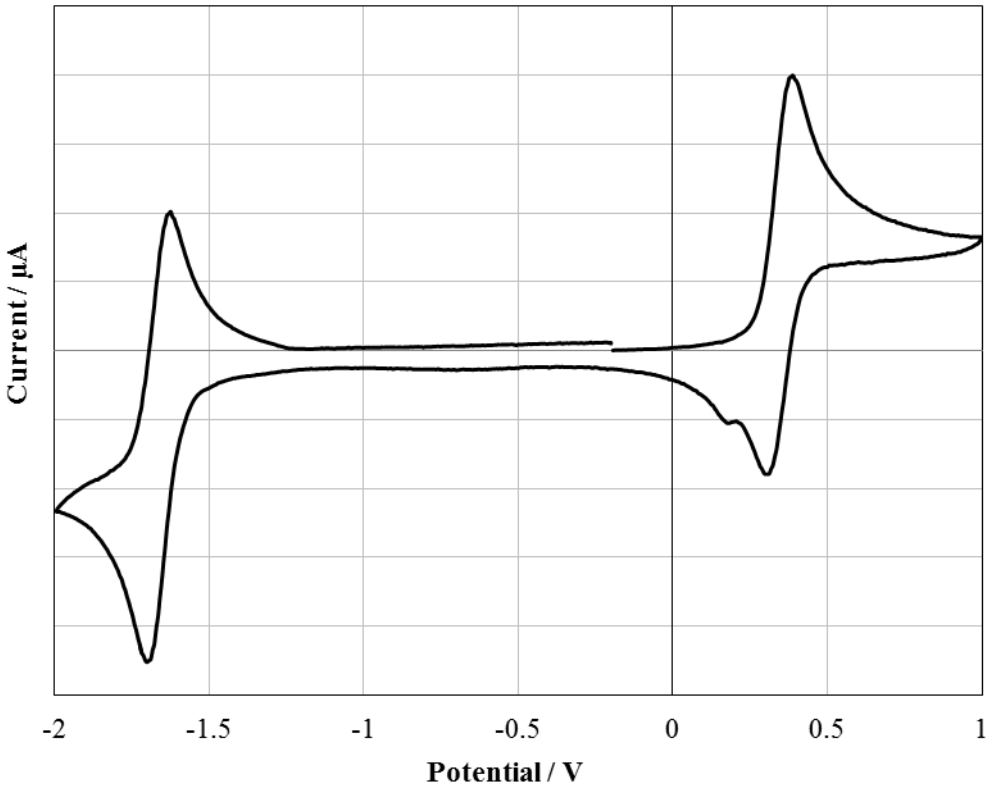

Figure S50. Cyclic voltammogram of $[Ni^{II}L^{Pr}](BF_4)$ **before** carrying out a controlled potential coulometry experiment at -1.80 V as 1 mmol L^{-1} solutions in MeCN (100 mV s^{-1}, 0.1 mol L^{-1} NEt_4PF_6, platinum electrode, versus 0.01 mol L^{-1} $AgNO_3$/Ag).

Mass of $[Ni^{II}L^{Pr}](BF_4)$ used = 4.6614 mg

Concentration of $[Ni^{II}L^{Pr}](BF_4)$ = (0.0046614) / (0.010 x 464.92) =1.000 x 10^{-3} mol L^{-1}

The expected number of electrons to be transferred provided that this particular process was a one electron process was calculated to be0.97 coulombs. This was calculated from the following equation.

No. of moles of $[Ni^{II}L^{Pr}](BF_4)$ = Concentration of $[Ni^{II}L^{Pr}](BF_4)$ x Volume
= 0.00100 Mol L^{-1} x 0.010 L
= 0.00001 mol

No of electrons transferred = n_e x No. of moles of $[Ni^{II}L^{Pr}](BF_4)$ x Faraday's constant
= 1 x 0.00001 mol x 96500 C mol^{-1}
= 0.965 C if one electron process

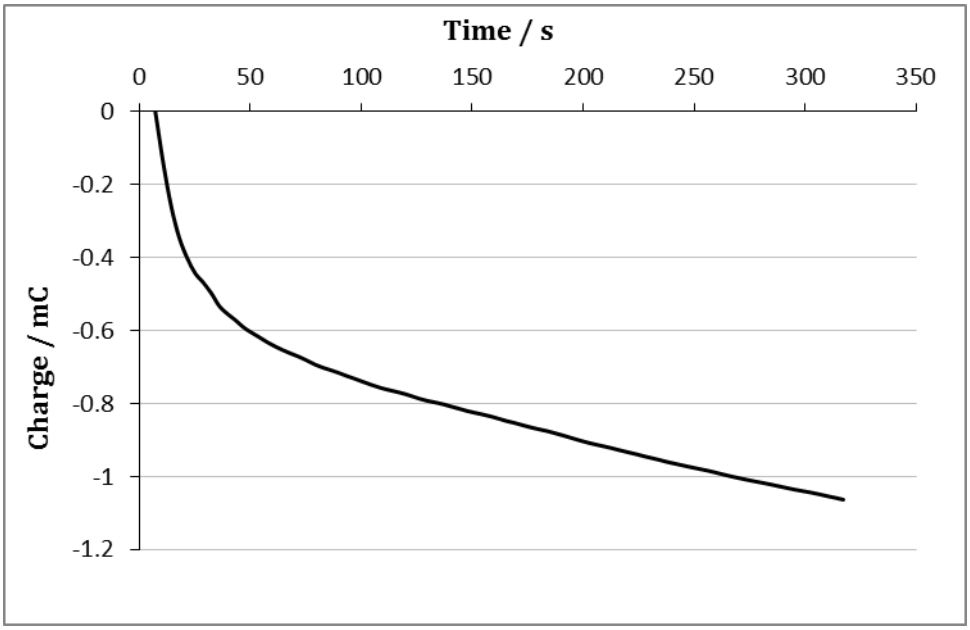

Figure S51. Controlled potentiostatic coulometry experiment conducted at -1.80 V led to 1.1 coulombs of electrons transferred which corresponds to 1.13 electron equivalents per complex.

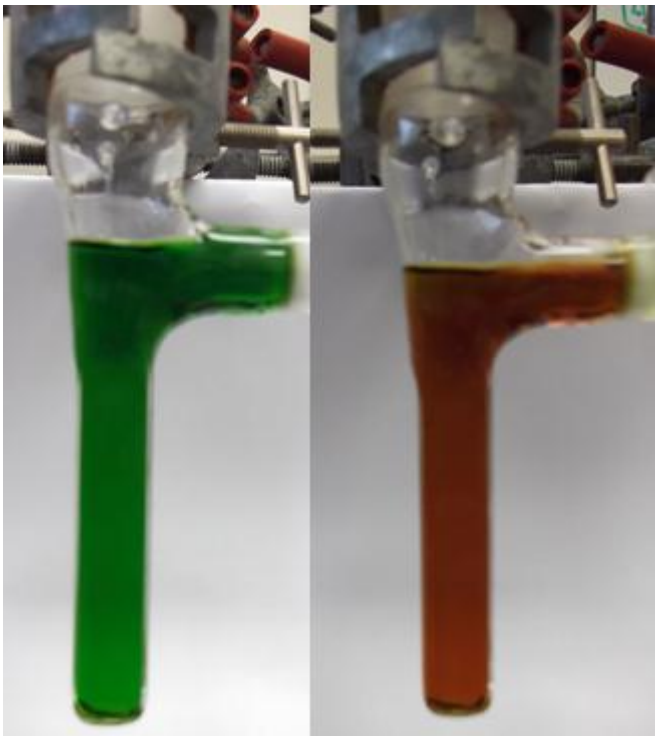

Figure S52. A significant colour change is observed upon controlled potential coulometry experiment at -1.8 V for $[Ni^{II}L^{Pr}](BF_4)$ which resulted in the transfer (removal) of 1.1 electron equivalents. Left: before; Right: after.

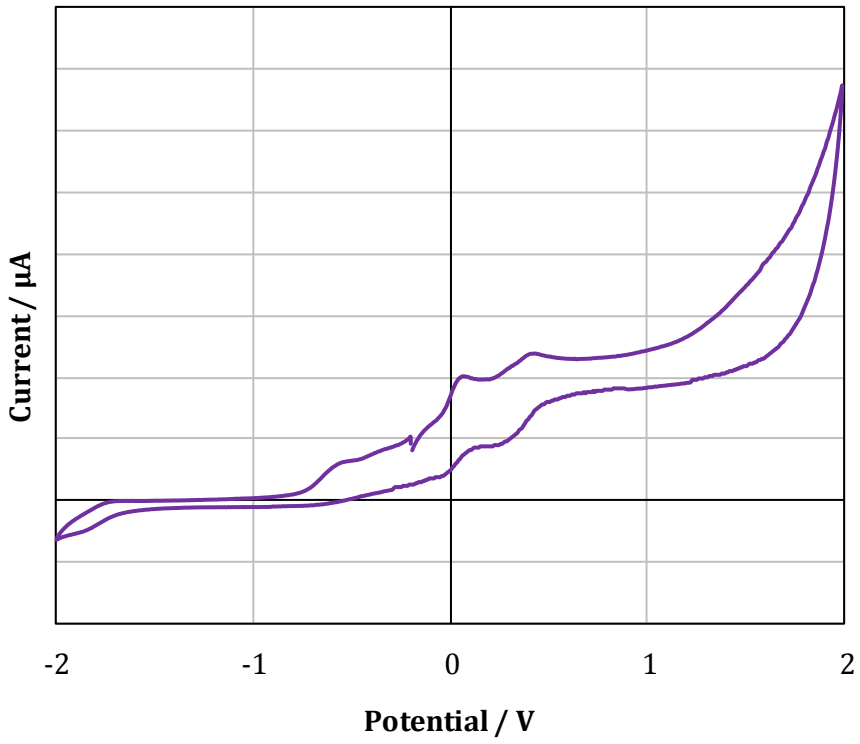

Figure S53. Cyclic voltammogram of $[Ni^{II}L^{Pr}](BF_4)$ **after** carrying out a controlled potential coulometry experiment at -1.80 as 1 mmol L^{-1} solutions in MeCN (200 mV s^{-1}, 0.1 mol L^{-1} NEt_4PF_6, platinum electrode, versus 0.01 mol L^{-1} $AgNO_3$/Ag).

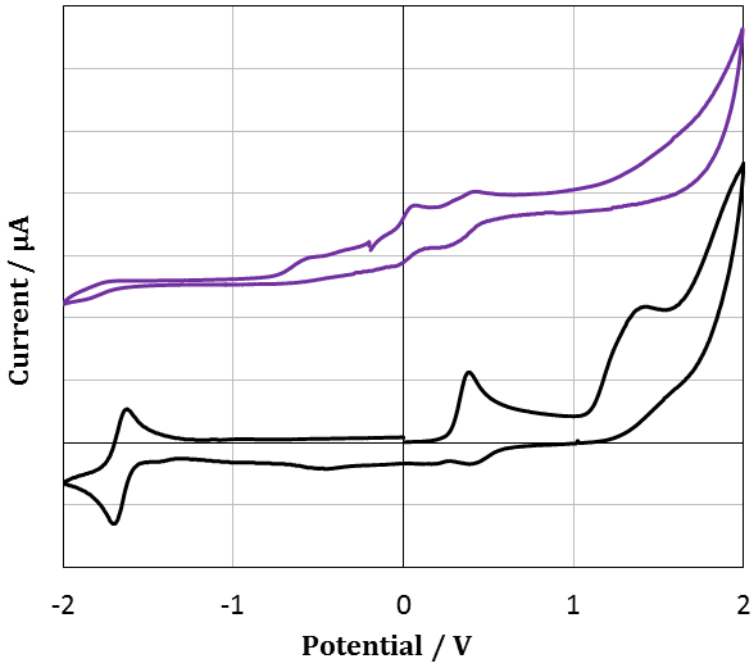

Figure S54. Cyclic voltammogram, from the bottom of $[Ni^{II}L^{Pr}](BF_4)$ **before** (purple) and **after** (red) carrying out a controlled potential coulometry experiment at -1.80 as 1 mmol L^{-1} solutions in MeCN (200 mV s^{-1}, 0.1 mol L^{-1} NEt_4PF_6, platinum electrode, versus 0.01 mol L^{-1} $AgNO_3$/Ag).

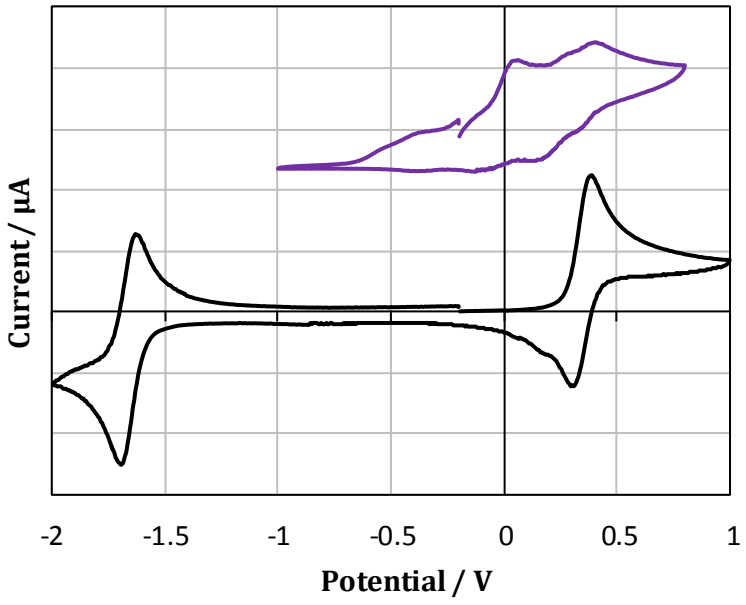

Figure S55. Cyclic voltammogram, from the bottom of $[Ni^{II}L^{Pr}](BF_4)$ **before** (purple) and **after** (red) carrying out a controlled potential coulometry experiment at -1.80 as 1 mmol L^{-1} solutions in MeCN (200 mV s^{-1}, 0.1 mol L^{-1} NEt_4PF_6, platinum electrode, versus 0.01 mol L^{-1} $AgNO_3$/Ag).

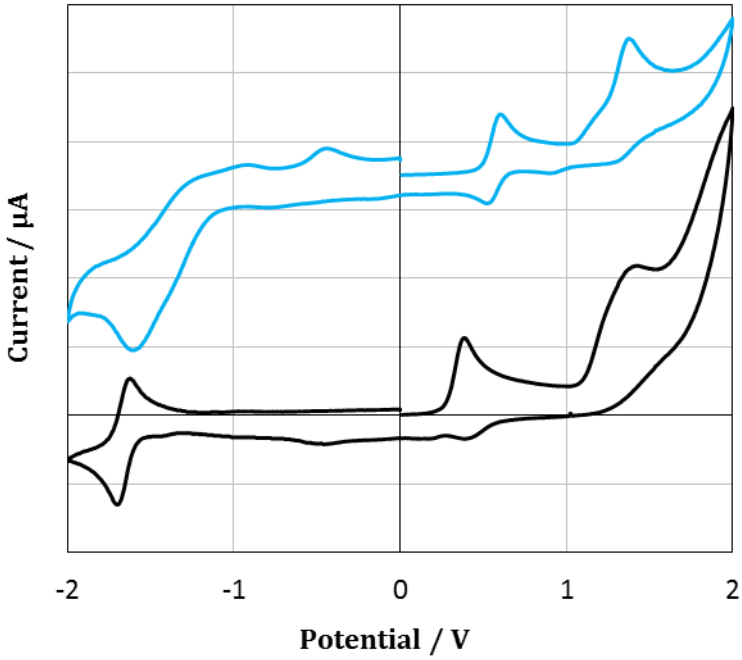

Figure S56. Comparison of the CVs of from bottom to top for $[Ni^{II}L^{Pr}](BF_4)$ (black) and $[Ni^{II}L^{Et}](BF_4)\bullet H_2O$ (blue) **before** carrying out a controlled potential coulometry experiment as 1 mmol L^{-1} solutions in MeCN (200 mV s^{-1}, 0.1 M NEt_4PF_6, platinum electrode, versus 0.01 M $AgNO_3$/Ag).

Electrochemical study $[Co^{II}L^{Pr}](BF_4)\bullet 0.5H_2O$ in MeCN

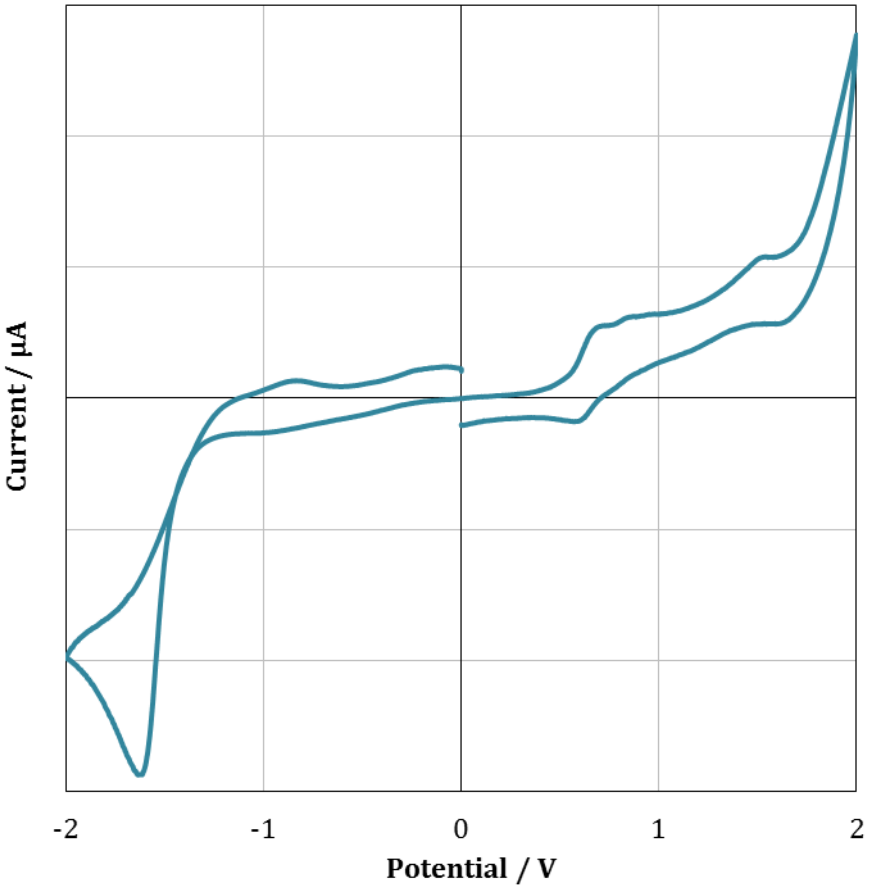

Figure S57. Cyclic voltammogram of $[Co^{II}L^{Pr}](BF_4)\bullet 0.5H_2O$ as 1 mmol L^{-1} solutions in MeCN (100 mV s^{-1}, 0.1 mol L^{-1} NBu_4PF_6, platinum electrode, versus 0.01 mol L^{-1} $AgNO_3$/Ag).

No controlled coulometry experiment was carried on this complex.

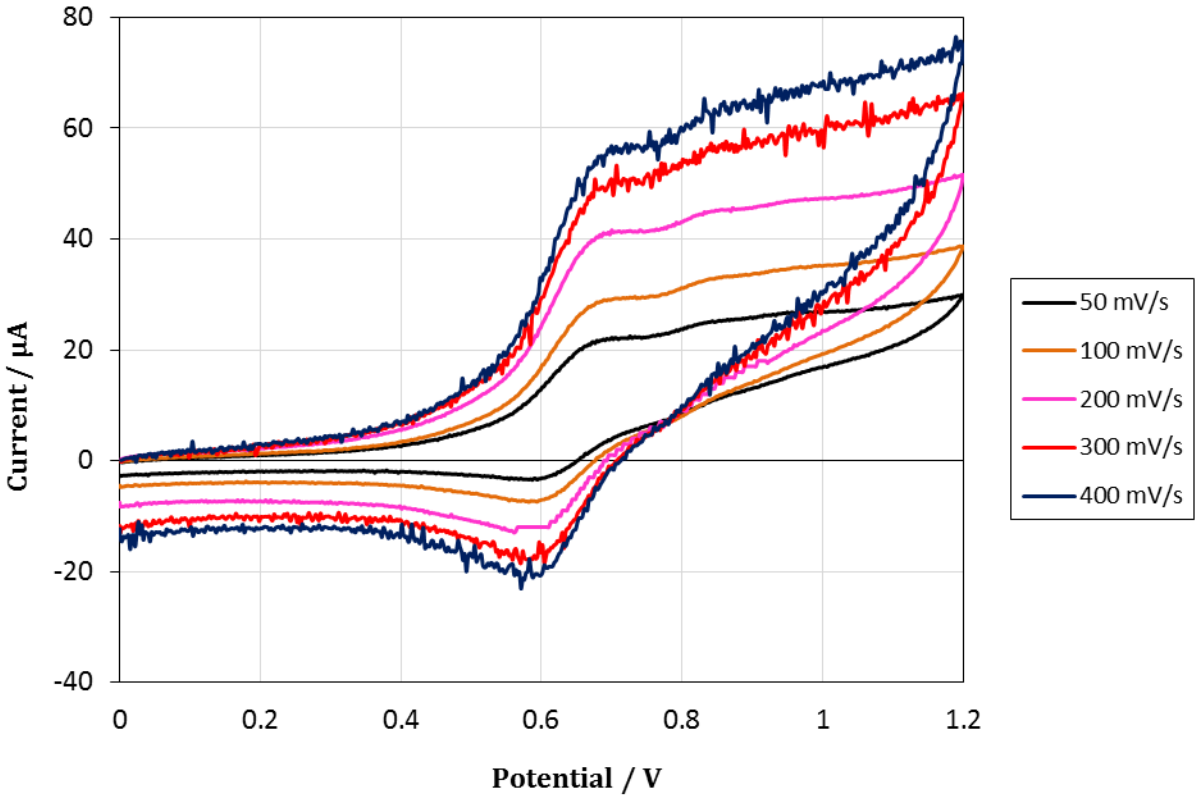

Figure S58. Cyclic voltammogram of $[Co^{II}L^{Pr}](BF_4)\bullet 0.5H_2O$ (oxidation process) at different scan rates (mV s^{-1}) as 1 mmol L^{-1} solutions in MeCN (0.1 mol L^{-1} NEt_4PF_6, platinum electrode, versus 0.01 mol L^{-1} $AgNO_3$/Ag).

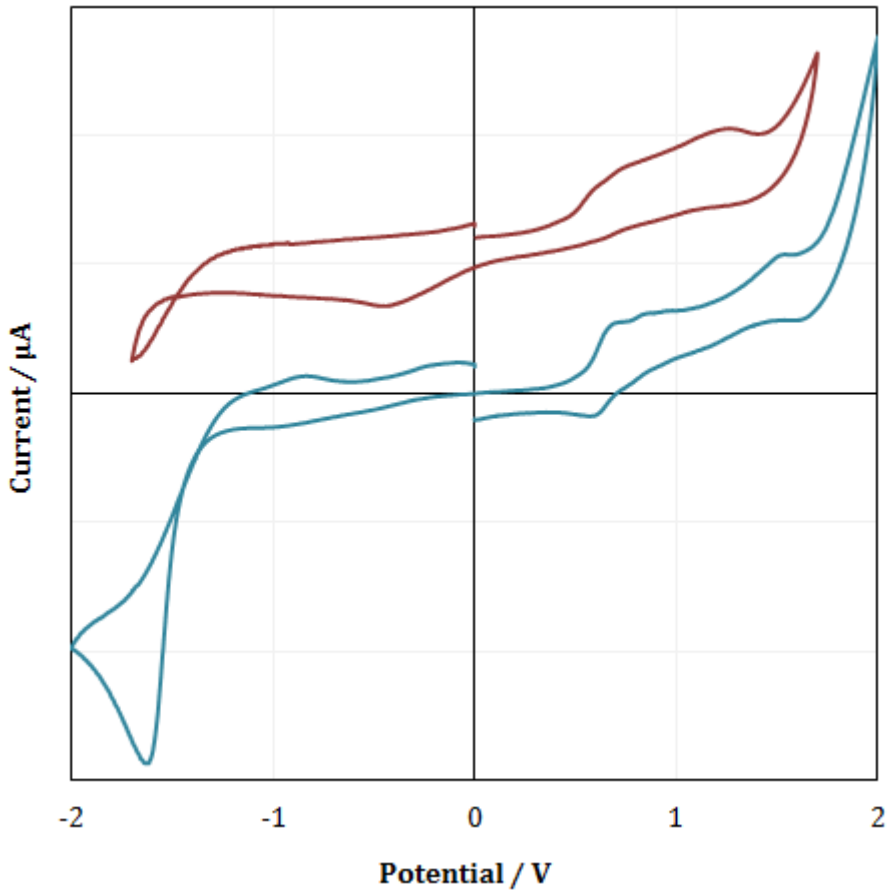

Figure S59. Comparison of the CVs of from bottom to top for $[Co^{II}L^{Pr}](BF_4)\bullet 0.5H_2O$ (blue) and $[Co^{II}L^{Et}](BF_4)\bullet H_2O$ (blue) as 1 mmol L^{-1} solutions in MeCN (200 mV s^{-1}, 0.1 M NEt_4PF_6, platinum electrode, versus 0.01 M $AgNO_3$/Ag).

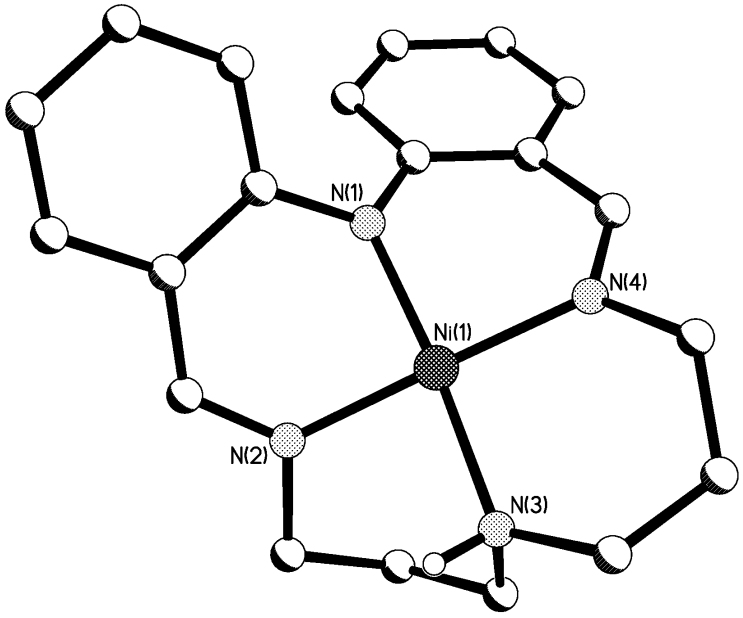

Figure S60. Perspective view of the cation of $[Ni^{II}L^{Pr}](BF_4)$. Non acidic hydrogen atoms and tetrafluoroborate anion omitted for clarity.

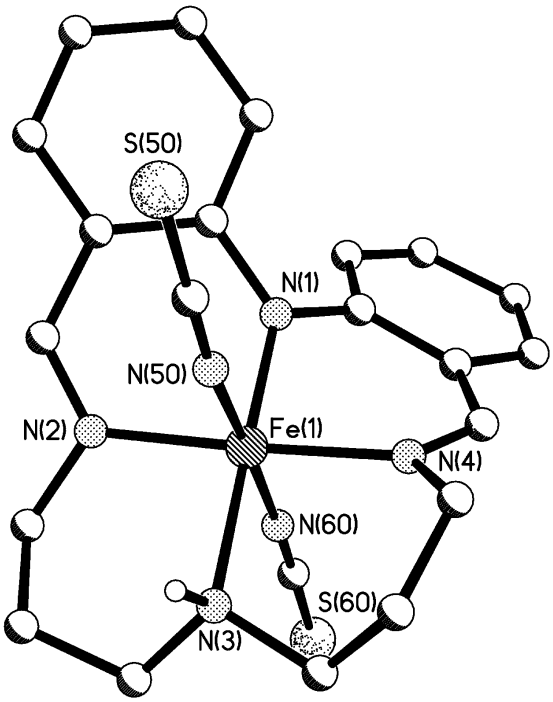

Figure S61. Perspective view of one of the two independent molecules of $[Fe^{III}L^{Pr}(NCS)_2]$•0.15MeOH•0.2H_2O. Non acidic hydrogen atoms and solvent of crystallization omitted for clarity.

Detailed Structural Analysis of $[Ni^{II}L^{Et}](BF_4)$ and $[Ni^{II}L^{Pr}](BF_4)$

At first glance, the structures of $[Ni^{II}\mathbf{L}^{Et}](BF_4)$ and $[Ni^{II}\mathbf{L}^{Pr}](BF_4)$ appear to have approximate C_2 symmetry through N(1), Ni(1) and N(3) (Figure S60, S62-S63) however a more careful analysis reveals that in both structures the two "sides", phenyl-ring-A-N(2)-N(3) versus phenyl-ring-B-N(4)-N(3) are significantly different from each other. These differences, between the two "sides", are summarised in Tables S13 and S14 and highlighted in Figures S62 and S63.

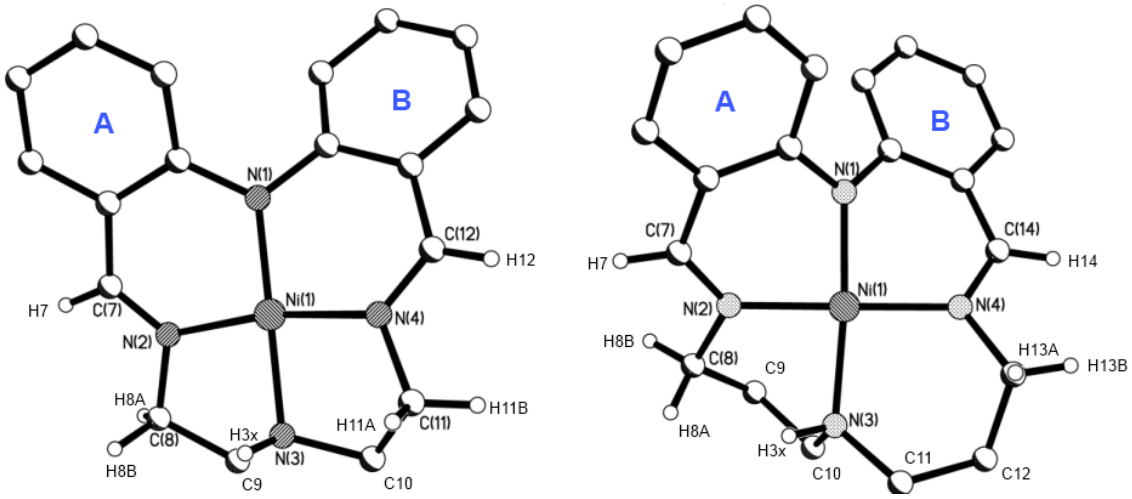

Figure S62. View of the two nickel structures (left) $[Ni^{II}\mathbf{L}^{Et}](BF_4)$ and (right) $[Ni^{II}\mathbf{L}^{Pr}](BF_4)$ with the N_4 mean plane in the plane of the page and just the hydrogen atoms referred to in Table S14 present and labelled. This highlights the off centre location of the N3 proton and the asymmetry of the side A *vs.* side B alkyl chains.

This more careful structural analysis (Tables S13 and S14, Figures S62 and S63) shows that these two nickel(II) complexes are not as symmetrical as they first appear. Rather, the two sides, A and B, are significantly different in the solid state. This is entirely consistent with the NMR studies in CD_3CN, in which there is a signal for every single proton in both of the alkyl chains. The situation for the aromatic proton signals differs for the two complexes: in the case of $[Ni^{II}\mathbf{L}^{Et}](BF_4)$ only 4 signals are observed in the aromatic region whereas in the case of $[Ni^{II}\mathbf{L}^{Pr}](BF_4)$ 8 signals are observed. This implies that the aromatic protons in $[Ni^{II}\mathbf{L}^{Et}](BF_4)$ are symmetrical whereas the ones in $[Ni^{II}\mathbf{L}^{Pr}](BF_4)$ are not. The greater difference between the alkyl chains on each side seen in structure of the $(\mathbf{L}^{Pr})^-$ complex than in the $(\mathbf{L}^{Et})^-$ complex (Table S13) likely renders the protons on the attached phenyl rings in the $(\mathbf{L}^{Pr})^-$ complex inequivalent. These differences are presumably due to the presence of the phenyl ring twist in combination with the H3x proton on N(3) which may be positioned up or down relative to that twist, and points slightly towards the raised phenyl ring.

Table S13. Structural comparison of the distances out of the plane of the attached phenyl ring and of the N_4-donor plane for $[Ni^{II}\mathbf{L}^{Et}](BF_4)$ and $[Ni^{II}\mathbf{L}^{Pr}](BF_4)$.

Atoms Side A/ side B	**Distance out of plane of attached phenyl ring / Å**	**Distance out of N_4-donor plane**
$[Ni^{II}L^{Et}](BF_4)$		
C7/12 (Schiff-base)	0.136/0.182	0.248/0.294
N2/4 (Schiff-base)	0.410/0.437	0.009/0.009
C8/11	0.628/0.669	0.514/0.250
C9/10	0.804/1.812	0.691/0.442
$[Ni^{II}L^{Pr}](BF_4)$		
C7/14 (Schiff-base)	0.066/0.050	0.514/0.674
N2/4 (Schiff-base)	0.280/0.230	0.069/0.064
C8/13	0.001/0.080	0.898/0.582
C9/12	0.075/1.066	1.926/0.203
C10/11	1.298/1.445	1.280/0.697

Table S14. Structural comparison of the distance of the side A / side B Schiff-base hydrogen atoms (H7/12 and H7/14) from the hydrogen atoms on the neighbouring alkyl carbon atoms (C8 and either C11 or C13) in $[Ni^{II}\mathbf{L}^{Et}](BF_4)$ and $[Ni^{II}\mathbf{L}^{Pr}](BF_4)$.

$[Ni^{II}L^{Et}](BF_4)$	**Distance / Å**
H7 (Schiff-base)…H8A/B	2.429/2.595
H12 (Schiff-base)…H11A/B	2.979/2.218
$[Ni^{II}L^{Pr}](BF_4)$	
H7(Schiff-base)…H8A/B	2.727/2.307
H14 (Schiff-base)….H13A/B	3.038/2.046

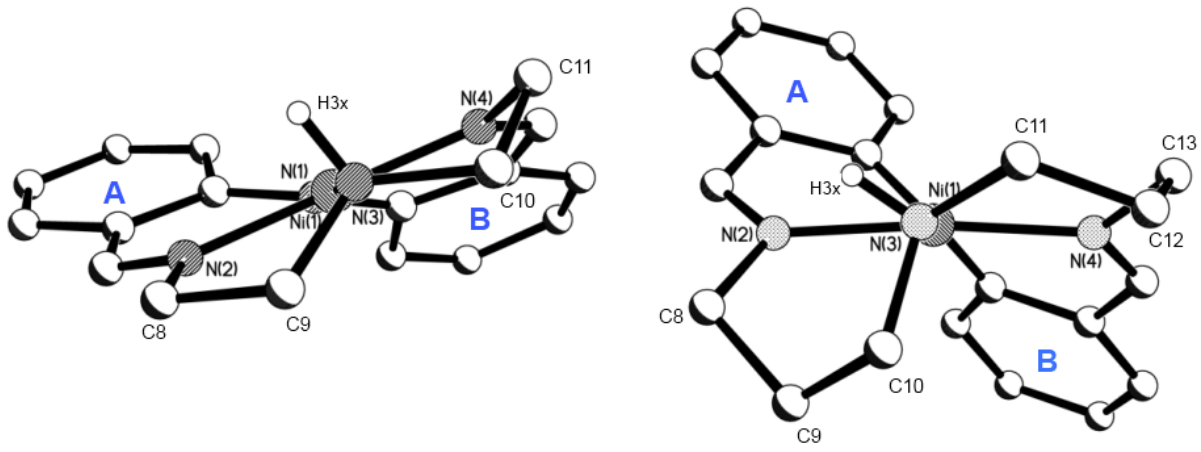

Figure S63. Comparison of the two nickel structures viewed at right angles to the N_4 mean plane (and hence perpendicular to the views shown in Figure S62) looking down the N(1)-Ni(1)-N(3) bond, (left) $[Ni^{II}\mathbf{L}^{Et}](BF_4)$ and (right) $[Ni^{II}\mathbf{L}^{Pr}](BF_4)$.